

Formulation of the Anisotropic Coarsening Theory and Applications to the Liquid-Phase Sintering of Si_3N_4

by
Trisha Salagaram

Submitted in partial fulfillment of the requirements
for the degree of Master of Science in the
School of Chemical and Physical Sciences
University of Natal

Pietermaritzburg
December 2002

Declaration

I declare that this work is a result of my own research, except where specifically indicated to the contrary, and has not been submitted for any other degree of examination to any other university.

Signed: T Salagaram

Date: 18 - 02 - 2003

Abstract

We have developed a new coarsening theory that more completely describes grain growth of a system of anisotropic particles such as completely faceted crystals by Ostwald ripening. Our model takes the anisotropy of surface energies on dissimilar facets into account, and the particle sizes are described by a distribution function. The theory is applied to study the coarsening of β -silicon nitride in a liquid medium due to the anisotropic growth of grains in different crystallographic directions. A model of the growth of silicon nitride grains is obtained based on the numerical solution of the equations of the new theory.

Computer experiments are performed to determine how the distribution function evolves, to investigate the influence of various parameters such as diffusion and interfacial reaction constants on grain growth and to extract grain growth exponents from this model in order to determine the growth mechanisms that are responsible for the anisotropic growth behaviour. Only preliminary numerical results are available thus far due to $1/r$ instabilities that occur in the theory as $r \rightarrow 0$.

Contents

Declaration	i
Abstract	ii
Contents	iii
List of Symbols	vi
1 Introduction	1
2 State of the Art	6
2.1 Consolidation of ceramic materials and grain growth	6
2.1.1 Powder processing	7
2.1.2 Shaping	8
2.1.3 Sintering	9
2.1.4 Finishing	14
2.1.5 Ceramic microstructure	15
2.2 Silicon nitride materials	16
2.2.1 Overview of the preparation and properties	17

2.2.2	Experimental features of grain growth in silicon nitride materials	24
3	Grain Growth Theories	28
3.1	The LSW theory	29
3.1.1	Solving the general isotropic problem in the limit of $t \rightarrow \infty$	38
3.2	Applications of grain growth theories to silicon nitride	42
4	Numerical Studies of the Isotropic System	47
4.1	Numerical solution to the isotropic problem in the diffusion and interfacial reac- tion controlled limits	48
4.2	Numerical solution of the general isotropic problem	50
4.3	Results and discussion	56
4.3.1	Numerical solution to the diffusion and interfacial reaction controlled limits of mass transfer	56
4.3.2	Numerical solution to the general isotropic problem	59
5	Anisotropic Coarsening Theory	66
5.1	Formulation of the anisotropic coarsening theory	66
5.2	Diffusion-controlled and interfacial reaction-controlled processes	81
5.3	Chemical isotropy and physical anisotropy	83
5.4	Comparison between the model developed by Kitayama <i>et al</i> and the anisotropic coarsening theory	84
6	Numerical Studies of the Anisotropic System	87
6.1	Numerical methodology	87

6.2	Results and discussion	90
6.2.1	Data used for modeling	90
6.2.2	Preliminary results for the anisotropic system	91
6.3	Future directions	95
7	Conclusions and Final Remarks	98
	Glossary	101
	Acknowledgements	111
	Resumé	112
	Bibliography	116

List of symbols

a	Lateral radius.
A_{001}	Area of a hexagonal facet.
A_{100}	Area of a prismatic facet.
c	Longitudinal radius.
c_o	Saturation concentration above a particle of radius r .
C	Concentration in the liquid medium.
C_r	Ideal concentration above a particle of radius r .
C'_r	Actual concentration above a particle of radius r .
C_s	Ideal concentration above a surface s .
C_s^o	Saturation concentration above a surface s .
C'_s	Actual concentration above a surface s .
D	Diffusion constant or coefficient.
E	Total surface energy of a hexagonal and a prismatic facet.
f	Particle size distribution function.
$g(t)$	A function of time.

$h(\rho)$	A function of the reduced radius.
J	Flux of material.
k_{001}	Interfacial reaction constant for the (001) facet.
k_{100}	Interfacial reaction constant for the (100) facet.
k_b	Boltzmann constant.
n	Number of moles in a particle.
\dot{n}_{001}	Rate of change of the number of moles from the (001) facet with time.
\dot{n}_{100}	Rate of change of the number of moles from the (100) facet with time.
N	Number of particles per unit volume in the system.
N_s	Number of lattice sites on a surface s
r	Radius of a spherical particle.
R	Universal gas constant.
T	Temperature in Kelvin.
V	Volume of a particle.
V_m	Molar volume.
β	$\frac{1}{RT}$
ϕ	Total volume of the solid particles in the system.
μ_s	Chemical potential of a surface s .
ρ	Reduced radius.
σ_s	Surface energy of a surface s .

Ω The volume of a growth unit.

Chapter 1

Introduction

Silicon nitride (Si_3N_4) ceramics exhibit excellent mechanical properties over a wide range of temperatures as well as good resistance to wear, corrosion and thermal shock. As a result, their potential for technological applications is high and they are used in a wide range of applications such as cutting tools, engine components, ball bearings, metal forming and processing devices and gas turbines. This makes Si_3N_4 ceramics one of the most important technical ceramics available with annual growth rates of approximately 10 % [1, 2].

The properties of ceramic materials depend on the microstructure that forms during the ceramic fabrication process and more importantly during sintering of the ceramic powder compacts. Si_3N_4 ceramics are produced by liquid-phase sintering of powder compacts. The powders are composed of particles of the α - Si_3N_4 crystal modification (which is the major component of most Si_3N_4 powders), particles of the β - Si_3N_4 crystal modification and a small amount of sintering additives which are additional compounds that are necessary to produce dense Si_3N_4 ceramics.

At the sintering temperatures the additives form a liquid medium around the particles, and α - Si_3N_4 which is unstable at these high temperatures dissolves into the liquid medium and reprecipitates onto the large, stable β - Si_3N_4 particles. After the α to β transformation, the β - Si_3N_4 particles grow anisotropically by Ostwald ripening into elongated, needle-like grains. The aspect ratio of these grains is comparable to that of whiskers and this is the basis of *in situ* fibre-reinforcement of Si_3N_4 ceramics which is responsible for the high fracture toughness and strength which these ceramics exhibit. After sintering the liquid medium formed by the sintering additives forms a glassy silicate phase which may be crystalline or amorphous around the Si_3N_4 grains. This is referred to as grain boundary phase, and it influences the high temperature properties and fracture toughness of the ceramics.

The formation of the needle-like microstructure during sintering of Si_3N_4 depends on sintering parameters such as the type and amount of sintering additive, the amount and size of β nuclei present in the starting powders, the sintering times and temperatures and the annealing times and temperatures. The experimental aims of sintering Si_3N_4 (and most other ceramics) are concerned with achieving maximal densities, increasing aspect ratios to improve mechanical properties and to achieve a narrow distribution of grain sizes. The ability to reproduce favourable microstructures in the ceramics industry is determined by the ability to control the evolution of microstructure during the ceramic fabrication stages, and increasing demands on the requirements of the ceramic materials imply that more accurate control over microstructural evolution is required. In order to achieve this, a fundamental understanding of the grain growth mechanisms which are responsible for producing the desired microstructure must be understood.

It is well known that Ostwald ripening is responsible for the elongated, needle-like grains which characterise the microstructure of Si_3N_4 ceramics, and that this grain shape is determined by the kinetics of grain growth, that is, the needle-like grain shape is not an equilibrium grain shape. Therefore, the formation of this grain shape may only be understood on the basis of growth mechanisms.

Despite intensive investigations of Si_3N_4 ceramics, tailoring of the microstructure, which determines the properties, is based mostly on empirically determined principles [1]. This is due to the fact that the existing models of grain growth have at best provided a qualitative understanding of the process.

During the early 1960's, a quantitative theory describing Ostwald ripening, known as the LSW theory [3, 4], was developed for a dilute dispersion of spherical particles in a medium. As a result, it does not adequately describe Ostwald ripening in a system of anisotropic particles such as completely faceted crystals. The existing theories of grain growth are based on isotropic surface energies and growth mechanisms. This means that these theories are also unable to give an adequate description of the anisotropic growth of Si_3N_4 materials due to the anisotropic growth of grains in different crystallographic orientations [1]. Even recent models [5] of grain growth are unable to account for the anisotropic growth in fine β - Si_3N_4 materials after the α to β phase transformation [1]. Thus a more detailed model of the system based on the physics and chemistry of the growth behaviour and numerical solutions of the basic equations of the model is required.

A new anisotropic coarsening theory has been formulated which describes grain growth in an anisotropic system of particles. It is a generalisation of the LSW theory by Wagner [4]. The anisotropic coarsening theory is a general theory that is based on a diffusion process, and the basic equations of the theory must be solved selfconsistently in order to describe the growth behaviour of an anisotropic system of particles. It is applicable to the liquid-phase sintering of materials such as Si_3N_4 , silicon carbide (SiC) and diamond.

Although recent work by Kitayama *et al* [5] has made advances in the understanding of grain growth behaviour of $\beta\text{-Si}_3\text{N}_4$, our formulation of the anisotropic coarsening theory is more realistic since we take into account, for example, the anisotropy in the surface energies on dissimilar crystal facets, a distribution function is included to describe the evolution of particle sizes and a numerical solution of the basic equations makes it possible to go beyond a linear dependence of the interfacial reaction rate on the concentration gradients.

In this thesis, the anisotropic coarsening theory is developed and applied to a system of hexagonal Si_3N_4 particles with the aim of modeling the anisotropic growth of the Si_3N_4 grains based on the numerical solutions of the basic equations describing the anisotropic growth model. The aims of the project are to determine the numerical methods necessary for a stable solution to the anisotropic problem by first conducting a comprehensive numerical investigation of the LSW theory, and to apply the numerical methods to study the anisotropic system in detail. Computational experiments are conducted to investigate the effects of the system variables such as interfacial energies, diffusion and interfacial reaction constants and saturation concen-

trations on the evolution of the particle size distribution function and the evolution of grain aspect ratios. Growth exponents are also extracted from this model in order to determine the grain growth mechanisms responsible for the anisotropic growth of Si_3N_4 grains.

The knowledge and understanding of the grain growth behaviour in Si_3N_4 gained from the numerical solution of the anisotropic coarsening theory may be used for the tailoring of the microstructure of Si_3N_4 ceramics.

Chapter 2

State of the Art

2.1 Consolidation of ceramic materials and grain growth

Most technical ceramics are produced by sintering moulded ceramic powders. The ceramic fabrication process consists of few basic stages, namely, powder processing, shaping and sintering which are common to the majority of the ceramic consolidation methods [2, 6, 7, 8]. The techniques used in each of these stages are well known in the ceramics industry.

The goal of the ceramic fabrication process is to be able to produce a ceramic with the desired microstructure and density which develops when the powder is consolidated and sintered. Microstructure is the structure of the ceramic sample that is visible with the aid of microscopes such as the scanning electron microscope. It determines the physical properties of the ceramic such as strength, fracture toughness, wear resistance and high temperature properties. Therefore every step of the fabrication process, which has the potential to introduce microstructural flaws in the ceramic, has to be carried out with extreme caution and precision so that the

desired microstructure may be obtained. More importantly, a fundamental understanding of each step in the fabrication process is required if fine control over microstructural evolution during consolidation is to be achieved.

2.1.1 Powder processing

The characteristics of a ceramic powder have a major influence on the microstructure that develops during shaping and sintering. Therefore the production of advanced ceramics requires powders with a fine particle size, a narrow particle size distribution, spherical or equiaxial particle shapes for amorphous or crystalline particles respectively, no agglomeration (see glossary) or soft agglomeration and high purity [9].

The starting materials of the ceramic fabrication process occur either naturally or may be synthesised by an appropriate chemical reaction. The material may be amorphous or polycrystalline. A powdered material consisting of particles with the desired shape and size is obtained either by grinding the starting material using various milling techniques or by chemical methods such as precipitation of particles from a solution. Other chemical methods are used to clean and de-agglomerate the particles.

Processing and sintering additives are mixed homogeneously into the powder by milling or chemical methods. The processing additives that are mixed with the powder are dispersants, binders, plasticisers and solvents. These are usually organic polymers, and their function is to ensure that the feed material (usually slurries or suspensions) required for subsequent shaping

have a uniform dispersion of the powder particles, no air bubbles and adequate viscosity. Processing additives are removed from the shaped body prior to sintering by a burnout process in which the shaped body is heated to temperatures at which these additives decompose. The burnout temperatures are well below sintering temperatures and the process is controlled so that no defects are introduced into the powder compact [2, 9].

Sintering additives are inorganic compounds that are added in very small quantities to ceramics. They are used to achieve high densities and control over grain growth during sintering. These additives usually form a second phase referred to as a grain boundary phase around the ceramic grains after sintering. Another class of sintering additives consists of those compounds that form solid solutions with ceramics. This means that ions from the sintering additive may be incorporated into the crystal structure of the host material. These are used to engineer alloys of ceramic materials with sintering additives which have specific property profiles.

2.1.2 Shaping

The processed powders may be moulded into various shapes by casting from a slurry (slip casting, tape casting), pressing methods (axial and isostatic pressing), plastic-forming methods (extrusion and injection moulding) and colloidal methods [9].

The processing additives in the powder help prevent defects from forming during shaping by ensuring that the feed material for shaping has a uniform distribution of particles, a suitable viscosity, plasticity and flexibility so that the result has a uniform density and a homogeneous

microstructure.

The shaped, unsintered object is referred to as a green body. If the preceding steps were carried out perfectly then the green body should have a homogeneous structure which is built up by the homogeneous packing of the processed powder particle mixture. The density of a green body may be between 50 and 70 % of the theoretical density. Therefore, an image of the microstructure should have a homogeneous distribution of particles and pores which are the spaces between particles in the green body. High green densities are often desired since this improves the densification rates and reduces sintering times.

There is an emphasis on homogeneity in the properties of the green body such as particle packing and arrangement, pore distribution and density since variations in these properties within the green body gives rise to defects such as inhomogeneous microstructure and density within the ceramic during sintering. The final sintered sample exhibits variations in mechanical properties which makes the ceramic unreliable for use in structural and other applications.

2.1.3 Sintering

A green body is converted into a dense solid with the desired microstructure by a heat treatment known as sintering. Sintering causes the particles in the green body to bond together and increase in size by mass transfer. During this process, the final microstructure of the ceramic develops and most of the pores are eliminated as they are filled up with mass. The driving force for sintering is the reduction in the overall surface area which accompanies grain growth

and results in the reduction of the free energy of the system.

The redistribution of mass between particles occurs by diffusion and results in densification when mass fills up the pores between particles thus reducing the pore volume and increasing the average size of grains. The growth of grains without a reduction of the pore volume is referred to as coarsening. Coarsening may hamper densification if it dominates the early stages of sintering since it causes grain growth which reduces the driving force for densification. Therefore densification and coarsening are referred to as competing mechanisms because the latter reduces the driving force for sintering without increasing the density of the ceramic sample. If coarsening is the dominant grain growth mechanism then the ceramics obtained are porous. Ceramics with maximal densities may be obtained if densification is the dominant grain growth mechanism.

The sintering techniques used most frequently are pressureless sintering, gas pressure sintering, hot pressing and hot isostatic pressing (HIP). The apparatus used in each technique has a furnace in which the green body is heated. Sintering temperatures are usually approximately three quarters of the melting temperature of the ceramic material, for example, the melting point of Si_3N_4 which is not known exactly, but is in the range of 2300°C [1], is sintered at temperatures between 1200°C and 1500°C . In the latter two techniques, an external pressure is applied to the green body to enhance densification. The two most well-known types of sintering are solid-state sintering and liquid-phase sintering.

Solid-state sintering

In solid-state sintering, heating causes mass in the solid state to flow between particles by atomic diffusion. The powder does not melt and, therefore, this method is also referred to as dry sintering.

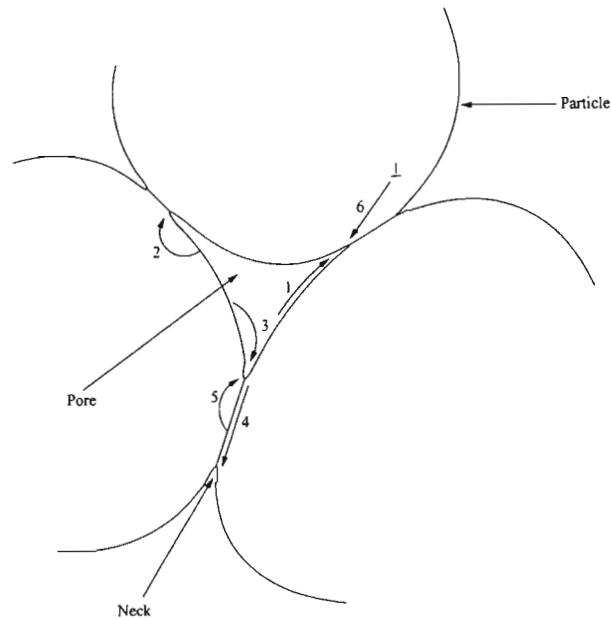


Figure 2.1: A diagram of solid-state sintering illustrating neck formation between contacting particles and the six mechanisms of mass transport between grains: (1) Surface diffusion, (2) Lattice diffusion from the surface, (3) Vapour transport, (4) Grain boundary diffusion, (5) Lattice diffusion from the grain boundary and (6) Plastic flow.

Particles in the compact are in contact with one another and the points of contact are referred to as necks. The surfaces of the particles and the neck are not flat. The chemical potential of the atoms on these two surfaces depends on the surface curvature. Convex surfaces have a positive radius of curvature and concave surfaces have a negative radius of curvature. As a result atoms on convex particle surfaces have a higher chemical potential compared to atoms on

the concave neck surfaces, and accumulate at the necks during sintering causing the particles to bond together and grow in size [9]. Six mechanisms of mass transport between particles have been identified: (1) surface diffusion, (2) lattice diffusion from the surface of a particle, (3) vapour transport, (4) grain boundary diffusion, (5) lattice diffusion from the grain boundaries and (6) plastic flow. All six mechanisms result in neck growth, however only the latter three mechanisms result in densification.

Grain boundaries in polycrystalline materials are characterised by grain boundary energies and grain boundary areas which may be likened to the surface (or interfacial) energies and surface areas associated with surfaces. Therefore changes in the grain boundary area contribute to the change in the free energy of the system, and this affects the driving force for sintering [9]. Grain boundaries also interact with pores which influences pore evolution during sintering. This interaction complicates the analysis and understanding of grain growth phenomena in polycrystalline materials. Therefore, most theoretical models of densification as a first approximation ignore pore and grain boundary dynamics [9]. The interaction between the mass transport mechanisms during sintering is also very complex, and existing models of sintering treat these mechanisms separately.

An external pressure is often applied to the green body during sintering to prevent coarsening from dominating grain growth. The external pressure increases the driving force for densification without affecting the coarsening rates [9]. In practice, solid-state sintering does not completely eliminate the pore volume and the microstructure of the ceramics consists of grains separated by grain boundaries.

Liquid-phase sintering

Ceramic materials with strong covalent bonds will not densify even with the application of external pressures to the green body during dry sintering. In fact, there are some material such as Si_3N_4 which decompose under these conditions of high temperatures and pressures. This is remedied by adding small amounts of sintering additives to the ceramic powders before shaping, which melt at the sintering temperatures thus forming a liquid which surrounds the particles. This is known as liquid-phase sintering. Mass diffuses more easily and faster through the liquid medium into the pores. Hence densification rates are enhanced in liquid-phase sintering.

If the amount of liquid material is sufficient and has good wettability, it fills the pores and exerts a capillary force on the particles which causes them to rearrange themselves into more stable, densely packed positions. This rearrangement process is responsible for a significant amount of densification and occurs in the first few minutes of sintering [9].

Atoms on the particle surfaces with a higher chemical potential will dissolve into the liquid, diffuse through it and precipitate onto surfaces with a lower chemical potential. This process is referred to as the solution-precipitation stage of liquid-phase sintering. The higher the curvature of a surface, the higher the chemical potential of that surface. In general, the smaller particles in the system have a higher chemical potential than the larger particles. Therefore, the smaller particles will tend to dissolve, and the smallest particles eventually disappear and re-precipitate onto the larger particles. The growth of the larger particles at the expense of the

smaller ones is known as Ostwald ripening. The solution-precipitation process is responsible for an increase in the average grain size of the system and for changes in grain shapes.

Once densification slows down, the final stage of liquid-phase sintering occurs during which grains increase in size by coarsening which occurs by Ostwald ripening. This stage is characterised by very little densification, an increase in the average size of the grains and grain shape accommodation which describes the movement of grains into more stable positions relative to one another.

The reduction of pore volume causes the compact to shrink during densification. The relationship between shrinkage rates and temperature provides information about which mechanisms dominate the sintering process, for example densification. This relationship is also used to determine the progress of the sintering process.

Upon cooling, the liquid phase in general forms a glassy grain boundary phase around the ceramic grains. The nature of the grain boundary phase influences the behaviour of the ceramic at high temperatures. Most ceramics undergo a post-sintering heat treatment or annealing to convert the amorphous grain boundary phases into crystalline phases.

2.1.4 Finishing

Finishing refers to polishing, cutting, grinding and drilling of the final product. This step is a means of ensuring that the ceramic applications satisfy the high requirements that are ex-

pected of technical ceramics. However it is expensive, and as the preceding steps in the ceramic fabrication are improved, the sintered ceramic applications will require less finishing. Diamond tools, laser cutting and spark erosion are examples of tools used for finishing.

2.1.5 Ceramic microstructure

The mechanical properties of a ceramic are controlled by the microstructure, namely grain size and shape, grain size distribution, grain boundary phases and density. Technical ceramics are used in industrial applications such as heat engines, cutting tools and bearings. Therefore they must exhibit excellent mechanical and wear properties consistently. This is only possible if the microstructure responsible for these properties is consistently reproduced by the ceramic fabrication process.

The use of different techniques at each stage of the fabrication process gives rise to a variety in the microstructures that may be obtained. In general, microstructural control is concerned with obtaining maximal densities (that is, approaching theoretical densities), small grain sizes, uniform particle size distributions and homogeneous microstructures since studies have shown that these factors are associated with reliable applications.

The parameters that influence the formation of microstructure during sintering are powder characteristics, the sintering time, the temperature, the heating rate, the sintering atmosphere and the externally applied pressure. Slight variations in any of the parameters often result in significant changes in the microstructure.

2.2 Silicon nitride materials

Silicon nitride has the chemical formula Si_3N_4 . The bonds between the silicon and nitrogen atoms are strong covalent bonds. Therefore it is only possible to produce fully dense Si_3N_4 ceramics by liquid-phase sintering.

Crystal structures

Si_3N_4 crystallises into three structures. The Si_3N_4 grains in the ceramics exist in the α and β hexagonal crystal structures, illustrated in the figure below.

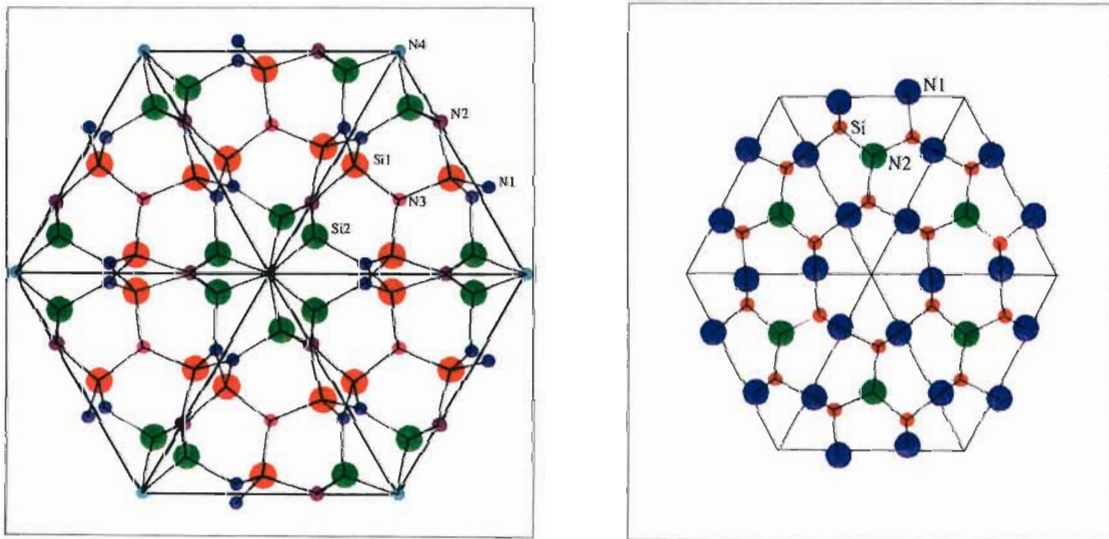


Figure 2.2: The α - and β - Si_3N_4 hexagonal crystal structures.

The building units of the hexagonal structures are SiN_4 tetrahedra. Each nitrogen atom is bonded to three silicon atoms which means that the tetrahedra connect at the corners forming a layer of Si_3N_4 . The β crystal structure consists of one such layer whereas the α crystal structure consists of two such layers, shifted with respect to one another. This results in a doubling of the c lattice parameter in the α - Si_3N_4 unit cell compared to that of the β -unit cell.

The third crystal structure of Si_3N_4 (produced only very recently at high temperatures and pressures) exists in a cubic, spinel crystal structure and is referred to as γ - Si_3N_4 in the literature. Studies of the γ -modification conducted to date [10, 11, 12] indicate that this material exhibits excellent mechanical properties making its potential for structural applications very high.

2.2.1 Overview of the preparation and properties

Powder synthesis and preparation

Silicon nitride does not occur naturally on earth, although inclusions of the material composed mainly of the α crystal structure have been found in meteorites [6, 2, 7]. Thus the starting materials for the fabrication process are synthesised via commercial chemical processes such as the direct nitridation of metallic silicon, carbothermal reduction of silicon dioxide (SiO_2) in nitrogen and high temperature decomposition of silicon diimide [13, 2, 14, 9, 7, 8]. The α modification of Si_3N_4 always forms the major component of the starting materials. The final product of the synthesis processes is, in general, a mass of large, agglomerated particles which

may be polycrystalline or amorphous depending on the synthesis route used [2, 6, 7, 8]. This is subsequently purified by various chemical methods [9], de-agglomerated and refined into a powder with the desired characteristics such as equiaxed particle morphology, high specific surface area, narrow particle size distribution by ball, planetary or attrition milling.

The starting materials produced by the different methods mentioned above differ from one another with respect to the amount of α - Si_3N_4 to β - Si_3N_4 present, crystallinity, particle morphology, amount of SiO_2 adhered to particle surfaces, agglomeration and impurities [2].

Processing and sintering additives are also mixed into the powder using the milling methods mentioned above. Other techniques [2, 9] may also be used to accomplish this. However, studies [2] have shown that the Si_3N_4 ceramics obtained from powders produced by milling are of a better quality compared to those obtained when other mixing techniques have been employed.

The processing additives such as dispersants, binders, solvents and plasticisers are added to the powder to produce a suitable feed material with a uniform distribution of Si_3N_4 particles, no bubbles and a suitable viscosity necessary for the subsequent shaping step. They are removed from the green body by burnout which is carried out very slowly to prevent defects from forming. Consequently, this process may take hours or even days to complete.

Sintering additives are a prerequisite for producing maximally dense silicon nitride ceramics. The types of compounds that have successfully yielded dense Si_3N_4 ceramics are mixtures of metal oxides such as Li_2O , CaO , MgO , SrO_2 , Al_2O_3 , ZrO_2 and Y_2O_3 or mixtures of metal

oxides with non-oxides such as AlN, ZrN and Mg₃N₂ [2, 7, 8].

Shaping

The choice of shaping technique depends on the requirements of the application of the ceramic.

Casting and injection moulding are used to generate shapes with complex geometries while

objects with simple geometries are produced by uniaxial and cold pressing methods [2, 7, 8].

Densification methods

Dense Si₃N₄ ceramics are obtained by liquid-phase sintering. Gas pressure sintering has proved to be the most economical sintering technique for producing Si₃N₄ ceramics and has had more success in reproducing favourable microstructures. Hot pressing (HP), hot isostatic pressing (HIP) and capsule hot isostatic pressing (capsule-HIP) are the other technologies that are used to densify Si₃N₄.

HIP is the only sintering technique that may be used to produce dense Si₃N₄ without sintering additives. The surface SiO₂ melts and often forms a sufficient amount of liquid around the particles during HIP-ing to densify the green body. However the use of HIP is more expensive compared to the other options and is used only to produce special applications.

Si₃N₄ ceramics are classified according to the sintering technique used. Therefore the types of Si₃N₄ ceramics that are manufactured are sintered Si₃N₄ (SSN), gas-pressure sintered Si₃N₄

(GPSN), hot pressed Si_3N_4 (HPSN), presintered hot isostatically pressed Si_3N_4 (HIP-SSN or Sinter-HIP SN) and encapsulated hot isostatically pressed Si_3N_4 (HIP-SN).

Finishing

Diamond tools are used to finish Si_3N_4 ceramics due to the hardness of the materials [2].

Densification mechanism

Dense Si_3N_4 may only be produced with the aid of sintering additives. The additives react with the SiO_2 , which exists naturally as a surface layer around particles, at the sintering temperature to produce a liquid which surrounds the particles in the system. This liquid provides a path for mass transfer between particles which results in dense Si_3N_4 .

Densification of Si_3N_4 starts at temperatures between 1200 and 1300 °C when the liquid formed infiltrates the pores between particles and causes particle rearrangement. The α - Si_3N_4 particles which are metastable at the sintering temperatures and the subcritical β -particles dissolve, diffuse through the liquid and re-precipitate on the larger, stable β -particles. This is referred to as the α to β transformation. After this transformation, the β particles grow anisotropically by Ostwald ripening yielding the elongated, needle-like β -grains which characterise the microstructure of Si_3N_4 ceramics. Densification continues as porosity is reduced by grain shape accommodation.

Upon cooling, the liquid forms an amorphous grain boundary phase around the particles. Annealing is often carried out to crystallise the grain boundary phase. However, a complete conversion has never been accomplished even for very long annealing times. Thus an amorphous glassy boundary phase is always present in these ceramics.

Microstructure and properties of silicon nitride materials

The properties that Si_3N_4 ceramics exhibit are due to the inherent characteristics associated with the hexagonal crystal structures and the microstructure that forms during sintering.

Si_3N_4 ceramics differ from one another with respect to grain morphology, composition and structure of the grain boundary phase and the degree to which α - and β -solid solutions are formed during sintering.

α - and β -solid solutions are formed when small amounts of the metal cations such as aluminium and beryllium, and oxygen anions occupy lattice sites in the Si_3N_4 crystal. The extent to which this occurs depends on the sintering additive and temperature [2]. The most well known Si_3N_4 solid-solutions are called SiAlON's. They are formed when Si^{4+} and N^{3-} ions are replaced by Al^{3+} and O^{2-} ions [13, 2, 7, 8]. In general, the microstructure of Si_3N_4 ceramics consists of hexagonal grains of β -solid solutions or α -solid solutions surrounded by an oxynitride glassy phase.

Si_3N_4 ceramics are known for their high strength, hardness and oxidation resistance over a

wide range of temperatures, high fracture toughness, fatigue strength, heat conductivity, corrosion resistance and good wear resistance. They are also light compared to other ceramics [13, 7, 8] due to the low density of Si_3N_4 .

The properties of high strength, hardness, fatigue strength and good wear behaviour at temperatures up to $1000\text{ }^\circ\text{C}$ [2] are associated with fine or needle-like grains and low additive content (where additive content refers to the amount of additive used for densification). The strength of the materials at these temperatures ranges between 800 MPa and 1400 MPa. The ceramics that contain α -solid solutions exhibit higher hardness than the materials in which the α - β transformation is complete. The hardness of β -solid solutions at high temperatures increases from 12 GPa to 16 GPa [13] as the amount of grain boundary phase and the average grain size decreases. The values of the hardness also depend on the technique used to measure them.

The mechanical properties of the ceramics at high temperatures, that is, temperatures greater than $1200\text{ }^\circ\text{C}$, are determined by the amount, composition and crystallinity of the grain boundary phase. Amorphous grain boundary phases begin to weaken at lower temperatures compared to crystalline grain boundary phases, and degrading phenomena such as creep, crack growth, corrosion and oxidation occur with more ease. Therefore Y_2O_3 and rare-earth oxides which produce crystalline grain boundary phases [15, 16] are used to engineer materials for high temperature applications while the use of Al_2O_3 , MgO and AlN are avoided. HIP-ed materials exhibit the best high temperature behaviour since low quantities of additives or no additives are required for densification.

High fracture toughness, heat conductivity and oxidation resistance are associated with large, coarse needle-like grains or large needle-like grains embedded in a matrix of fine grains. These properties are optimised when the additive content is low and free of Al_2O_3 . The microstructure consisting of elongated, needle-like $\beta\text{-Si}_3\text{N}_4$ grains and low additive content give rise to toughening mechanisms [2, 13] which increase the fracture toughness of the ceramics. Oxidation resistance depends on the surface layer of SiO_2 which forms around Si_3N_4 grains by oxidation. This layer hampers oxygen from diffusing into the grains thus reducing oxidation in this manner. Sintering additives react with SiO_2 to remove this protective layer consequently increasing the oxidation of the ceramics.

Si_3N_4 ceramics with fine grains and a low additive content are more resistant to wear or fatigue when exposed to cyclic pressures (or loads). Studies [13] have shown that wear resistance may be increased by using small amounts of titanium nitride (TiN) or boron nitride (BN) to form composites with Si_3N_4 [13].

The corrosion resistance of Si_3N_4 ceramics depends on the grain boundary phase, the SiO_2 content and temperature at which the ceramic materials are used. Studies [2, 13] have shown that Si_3N_4 materials corrode in hot acids under hydrothermal conditions and in bases. Resistance to corrosion increases as the temperature and additive content decrease. It has also been found that corrosion resistance in acids under hydrothermal conditions increases with an increase in the SiO_2 content, whereas corrosion resistance in bases decreases as the SiO_2 content in the ceramic increases.

The properties of the ceramics are also affected by defects that form during sintering. Pores, inclusions (formed by the reaction of impurities present in the starting powders with sintering additives and SiO_2), agglomerates of glasses, surface defects and even very large grains are all examples of defects that affect the physical properties of Si_3N_4 .

2.2.2 Experimental features of grain growth in silicon nitride materials

The microstructure of silicon nitride ceramics, in general, consists of elongated, needle-like grains surrounded by an oxynitride grain boundary phase.

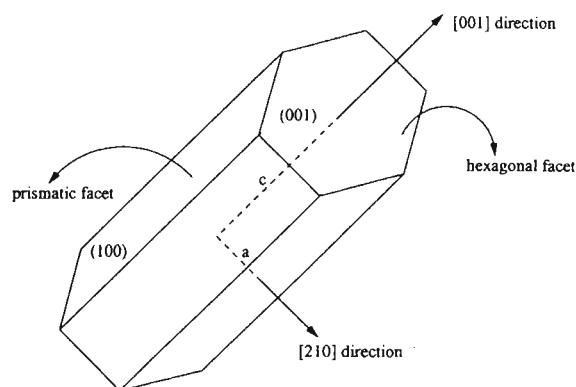


Figure 2.3: Diagram of a hexagonal $\beta\text{-Si}_3\text{N}_4$ particle illustrating the hexagonal and prismatic facets and the different crystallographic directions.

The needle-like grains form due to the anisotropic growth of grains along the c -axis of the $\beta\text{-Si}_3\text{N}_4$ particle. The ratio of grain length to grain width, referred to as the aspect ratio, is comparable to that of whiskers which gives rise to the phenomenon of *in situ* fibre-reinforcement

in Si_3N_4 ceramics, and is responsible for the materials' excellent mechanical properties such as strength and fracture toughness.

The anisotropic growth of $\beta\text{-Si}_3\text{N}_4$ grains occurs by Ostwald ripening during liquid-phase sintering of the ceramic powder compact. The presence of the liquid enhances diffusion and densification. The starting powders are usually rich in the α -phase which is thermodynamically unstable at the sintering temperatures and consequently transforms to the β -phase, which is stable at high temperatures. The instability of the α -phase causes the liquid phase to become supersaturated and, consequently, enhances the densification process as dissolved matter nucleates on the small fraction of β -particles resulting in the growth of rod-like β -grains [8]. Although it is well known that Ostwald ripening is responsible for the anisotropic grain growth in Si_3N_4 , there is no conclusive information about the mechanism of grain growth [5, 7]. This is to mean that growth exponents extracted from different theoretical models and experimental results indicate that grain growth is either controlled by diffusion through the liquid phase or by the reaction at the Si_3N_4 -liquid interface or both.

The anisotropic shape of the $\beta\text{-Si}_3\text{N}_4$ grains suggests that growth in the [001] direction occurs at a faster rate than growth in the [210] direction during sintering. Numerous experiments (laboratory and computer simulations) studying grain growth of silicon nitride have been carried out with the aim of resolving the question of the anisotropic grain growth mechanism.

Theoretical calculations [5, 17] have shown that the rod-like grain shape is the intrinsic growth shape of $\beta\text{-Si}_3\text{N}_4$. In addition, these calculations have predicted the growth of pyramid {101}

facets which have been observed experimentally [5]. The prediction and subsequent observation of these pyramid $\{101\}$ facets seems to imply that growth along the $[210]$ and $[001]$ directions are controlled by the reaction at the solid-liquid interface.

Estimations of the ratio of the surface energies of the two facets by the so called Broken Bond method have shown that the surface energy of the (100) facet is lower than that of the (001) facet. This requires more careful measurement and calculation. The surfaces of the crystal are not perfect, and surface defects provide sites where nucleation occurs. Assuming that the nucleation site on each facet has the same geometry as the crystal itself, the nucleation site on the hexagonal plane will have a lower chemical potential compared with the site on the prismatic plane. As a result, mass will tend to nucleate on the hexagonal nucleation sites causing growth to occur in the $[001]$ direction and elongated grains to form. Preferential growth in the $[001]$ direction means that the surface area of the facet with the lower surface energy, namely the (100) facet, increases and as a consequence of this, the grain attains the lowest possible free surface energy.

A study mentioned in reference [5] found that grain growth in the $[001]$ direction was controlled by diffusion while growth along the $[210]$ direction was controlled by the interfacial reaction. This could provide an explanation for the elongated grain shape since for such a situation, mass would diffuse from the prismatic plane onto the hexagonal plane resulting in immediate growth in the $[001]$ direction due to the rapid reaction at the (001) facet-liquid interface.

The observation of roughening on the hexagonal plane and the atomically smooth prismatic planes provides further evidence that growth on the hexagonal plane is controlled by diffusion and growth on the prismatic plane is controlled by the interfacial reaction. Diffusion of mass from the prismatic plane to the hexagonal plane can only occur one atom at a time. If the reaction at the interface occurs at a faster rate than diffusion, then growth of the hexagonal facet does not occur under equilibrium [17] and, as a result, this surface appears rough. Similarly, the slow reaction at the interface between the prismatic facet and the liquid compared to diffusion on this surface would account for this surface being atomically smooth.

It is evident from the findings of these studies that the mechanism of grain growth during liquid-phase sintering of Si_3N_4 is still under debate.

Chapter 3

Grain Growth Theories

The processes which occur during solid-state and liquid-phase sintering are complex and indistinguishable from one another. This makes the analysis of sintering very difficult and theoretical models of the interaction between the different mechanisms that occur during sintering have not yet been fully developed.

There are numerous methods used to study Ostwald ripening theoretically, such as analytical models, scaling laws, numerical simulations, topological models and statistical models. The analytical models have proved to be the most widely used technique and provides the basis for the present understanding of coarsening by Ostwald ripening [9]. These techniques use simple geometrical models to approximate the real systems (which are very complex in reality) and derive expressions for the growth rates based on these. Due to such simplifications, the analytical models have at best provided a qualitative understanding of the coarsening process.

Numerical analysis of coarsening is a relatively new field of research. It is not as widely used as

the analytical models because the calculations are complicated and the results are sometimes difficult to interpret [9]. The existing models are still far too simplistic, and do not provide adequate descriptions of the coarsening of microstructure by Ostwald ripening. Numerical analysis does, however, have the advantage that the systems may be studied without making drastic simplifications and more realistic models may be produced.

3.1 The LSW theory

During the early 1960's, a quantitative theory describing Ostwald ripening was developed independently by Lifshitz, Sloyosov, Wagner [3, 4] and Greenwood. The theory is generally known as the LSW theory and was developed for an isotropic system of spherical particles surrounded by a second medium. It does not adequately describe Ostwald ripening in a system of anisotropic particles such as completely faceted crystals [5, 3, 4].

In the analysis of Ostwald ripening by Wagner [4], the system is described in terms of a particle radius distribution function $f(r, t)$ which is defined as the number of particles per unit length with radii in the range r to $r + \Delta r$ at a time t [4]

$$f(r, t) = \lim_{\Delta r \rightarrow 0} \frac{N(r, r + \Delta r, t)}{\Delta r}. \quad (3.1)$$

It follows from the definition of $f(r, t)$ that the total number of particles in the system is

$$Z = \int_0^{\infty} f(r, t) dr, \quad (3.2)$$

the rate at which the particles disappear is

$$\frac{dZ}{dt} = \frac{d}{dt} \int_0^\infty f(r,t) dr = \lim_{r \rightarrow 0} (f\dot{r}), \quad (3.3)$$

and the total volume of solute in the system given by

$$\phi = \frac{4}{3} \pi \int_0^\infty r^3 f(r,t) dr, \quad (3.4)$$

is assumed to be conserved.

Using flux conservation, Wagner showed that eq.(3.1) satisfies the following continuity equation

$$\frac{\partial f}{\partial t} = - \frac{\partial}{\partial r} (f\dot{r}), \quad (3.5)$$

where \dot{r} is the rate at which a particle radius changes with time.

To solve the continuity equation (3.5), Wagner [4] required an expression for \dot{r} . Wagner [4] derived expressions for the rate of mass transfer from a particle due to diffusion

$$\dot{n} = - 4 \pi r D (C'_r - C), \quad (3.6)$$

where D is the diffusion constant, C'_r is the actual concentration above a particle and C is the concentration in the liquid medium, and the interfacial reaction

$$\dot{n} = - 4 \pi r^2 k (C_r - C'_r), \quad (3.7)$$

where k is the interfacial reaction constant and C_r is the ideal concentration above a particle. These rates (eq.(3.6) and eq.(3.7)) are equal in equilibrium yielding an expression for the actual concentration for C'_r and a general expression for mass transfer from a particle of radius r , that is

$$\dot{n} = - \frac{4\pi r^2 k D V_m}{kr + D} (C_r - C). \quad (3.8)$$

Since the change in the concentration of the liquid medium with time is negligible, Wagner [4] made the approximation that

$$\frac{\partial C}{\partial t} = - \int_0^{\infty} \dot{n}(r) f(r, t) dr \approx 0. \quad (3.9)$$

Substituting eq.(3.1) and eq.(3.8) into eq.(3.9) yields an expression for the concentration in the liquid medium C . A geometrical argument which relates the growth rate of a particle \dot{r} to the change in the volume of the particle with time is used to obtain an expression for \dot{r} :

$$\dot{r} = \frac{2\sigma C_o V_m^2}{rRT} \frac{kD}{kr + D} \left(\frac{r}{r^*} - 1 \right), \quad (3.10)$$

where r^* is defined as the radius of a particle in equilibrium with the liquid medium and is given by the expression

$$r^* = \int_0^{\infty} f(r, t) \frac{r^2}{kr + D} dr \Big/ \int_0^{\infty} f(r, t) \frac{r}{kr + D} dr. \quad (3.11)$$

All particles with radii smaller than r^* reduce their radii with time, with the smallest particles in the system disappearing altogether while the particles with radii greater than r^* grow at their expense. This is the phenomenon of Ostwald ripening.

Wagner solved the continuity equation (3.5) analytically for two special cases of diffusion controlled and interfacial reaction controlled mass transfer [3, 18, 4].

Diffusion controlled mass transfer ($D \ll kr$)

Wagner obtained an analytical solution to the continuity equation (3.5) in the diffusion controlled case in the limit of $t \rightarrow \infty$ [4]. In this limit, a finite number of particles disappear from

the system, therefore the distribution function has a finite value as $r \rightarrow 0$ and it follows that eq.(3.3) also has a finite value [4].

Considering particles with radii in the range $r \ll r^*$ it follows from eq.(3.10) that the rate at which a particle radius changes with time in the diffusion controlled case ($D \ll kr$) is

$$\dot{r} = \frac{-2 \sigma c_o V_m^2 D}{RT} \frac{1}{r^2}. \quad (3.12)$$

Substituting eq.(3.12) into eq.(3.3) yields the rate at which particles disappear from the system:

$$\frac{dZ}{dt} = \lim_{r \rightarrow 0} \left[f(r, t) \frac{-2 \sigma c_o V_m^2 D}{RT} \frac{1}{r^2} \right]. \quad (3.13)$$

Since the expression above has a finite value as $t \rightarrow \infty$ and $r \rightarrow 0$, it follows that $f(r, t)$ is proportional to r^2 as $r \rightarrow 0$.

Wagner assumed that after long observation times, it is possible to express the distribution function as a product of a pure function of time and a function of the reduced radius ρ , which is defined as

$$\rho = r/r^*(t). \quad (3.14)$$

The reduced radius is the ratio of a particle radius and the critical radius $r^*(t)$ which is itself a function of time. Since the left hand side of eq.(3.13) has a finite value under these conditions, Wagner assumed that $f(r, t)$ may be written as

$$f(r, t) = g(t) \rho^2 h(\rho), \quad (3.15)$$

where $g(t)$ is a function of time and $h(\rho)$ is a reduced radius distribution function. The value of $h(\rho)$ at $\rho = 0$ by definition is

$$h(\rho = 0) = 1. \quad (3.16)$$

It follows from substituting eq.(3.15) into eq.(3.11), and using eq.(3.14) to obtain an expression in terms of ρ , that $h(\rho)$ is required to satisfy the condition that

$$\int_0^\infty \rho^2 h(\rho) d\rho = \int_0^\infty \rho^3 h(\rho) d\rho. \quad (3.17)$$

Substituting eq.(3.15) into eq.(3.4) and using eq.(3.14) yields an expression for $g(t)$

$$g(t) = \frac{3\phi}{4\pi \int_0^\infty \rho^5 h(\rho) d\rho} \frac{1}{r^{*4}(t)}. \quad (3.18)$$

Substituting equations (3.12), (3.14) and (3.15) into eq.(3.3) and using eq.(3.18) to eliminate $g(t)$ from the resulting expression yields

$$\frac{dr^*}{dt} = \frac{2 \sigma c_o D V_m^2}{3 \gamma RT} \frac{1}{r^{*2}(t)}, \quad (3.19)$$

where

$$\gamma = \int_0^\infty \rho^2 h(\rho) d\rho. \quad (3.20)$$

Assuming that it is possible to express the distribution function in the separable form given by eq.(3.15) as $t \rightarrow \infty$ means that eq.(3.19) may be integrated to obtain an expression for r^* :

$$r^{*3}(t) = r^{*3}(0) \left[1 + \frac{t}{\tau} \right], \quad (3.21)$$

where

$$\tau = \frac{\gamma RT r^{*3}(0)}{2 \sigma c_o V_m^2 D},$$

is a constant with the dimensions of time.

Substituting equations (3.18) and (3.21) into eq.(3.15) yields the following expression for $f(r, t)$:

$$f(r, t) = \frac{\rho^2 h(\rho)}{\left(1 + \frac{t}{\tau}\right)^{\frac{4}{3}}} \times \text{const.} \quad (3.22)$$

Equations (3.22) and (3.12) are substituted into eq.(3.5). Using the approximation that $D \ll kr$ in the diffusion controlled case and the equations (3.14) and (3.21), the following differential equation is obtained:

$$(\gamma^{-1}\rho^3 - 3\rho + 3) \frac{dh}{d\rho} + (\gamma^{-1}\rho^2 - 3)h = 0. \quad (3.23)$$

Since time does not appear explicitly in the above equation, Wagner assumed that eq.(3.23) is an extension of the continuity equation (3.5) under steady state conditions in the diffusion controlled limit [4].

Wagner made further approximations to obtain a value of 9/4 for the parameter γ [4], and an expression for the reduced radius distribution function $h(\rho)$ is obtained by integrating eq.(3.23):

$$\begin{aligned} h(\rho \leq 3/2) &= \left(\frac{3}{3+\rho}\right)^{7/3} \left(\frac{3/2}{3/2-\rho}\right)^{11/3} \exp\left[-\frac{\rho}{3/2-\rho}\right], \\ h(\rho \geq 3/2) &= 0. \end{aligned} \quad (3.24)$$

Interfacial reaction controlled mass transfer ($kr \ll D$)

The same methodology is used to derive the expressions corresponding to the equations (3.12) to (3.24) for the interfacial reaction controlled case. The approximation $kr \ll D$ is made and the system is studied in the limit of $t \rightarrow \infty$ [4].

The expression that Wagner [4] obtained for r^* is [4]

$$r^{*2}(t) = r^{*2}(0) \left[1 + \frac{t}{\tau} \right], \quad (3.25)$$

where

$$\tau = \frac{3RT\gamma r^{*2}(0)}{4\sigma c_o V_m^2}.$$

and

$$\gamma = \int_0^\infty \rho h(\rho) d\rho,$$

In this limit the value of the parameter γ is $4/3$ and the expression for the reduced radius distribution function $h(\rho)$ is

$$\begin{aligned} h(\rho \leq 2) &= \left(\frac{2}{2-\rho} \right)^5 \exp \left[-\frac{3\rho}{2-\rho} \right], \\ h(\rho \geq 2) &= 0. \end{aligned} \quad (3.26)$$

The equations (3.21) and (3.25) are statements of the well known grain growth laws associated with the LSW theory [3, 4]. The exponents in these expressions are referred to as growth expo-

nents. Therefore according to Wagner's analysis, a particle radius has a cubic growth exponent for mass transfer controlled by diffusion and a quadratic growth exponent for the interfacial.

In both cases, Wagner found that when the final distribution function is scaled by the critical radius, the form of this scaled distribution function is universal, independent of the form of the initial distribution function. In the diffusion controlled case, the distribution function has a characteristic r^2 dependence close to the origin and in the interfacial reaction controlled case the dependence of $f(r, t)$ on r is linear close to the origin. These results were also obtained by Lifshitz and Sloyozov [3].

Shortcomings of the LSW theory

Although the LSW theory was an advance in the understanding of Ostwald ripening, it has several shortcomings:

1. The theory applies strictly to a dilute dispersion of spherical particles which means that there are no interparticle diffusion interactions.
2. Since interparticle distances are larger than the dimensions of a particle Wagner [4] assumed that the gradient of the concentration ∇C may be approximated by the difference between the actual concentration and the concentration in the liquid divided by the radius of a particle, that is, $\nabla C \approx (C'_r - C)/r$. This approximation is used to derive eq.(3.6). Such an approximation is unnecessary in a complete numerical solution of the problem.
3. The equations for mass transfer due to the interfacial reaction (eq.(3.7)) is obtained by

assuming that the rate of mass transfer due to the interfacial reaction is proportional to the surface area of a particle and to the difference between the ideal concentration C_r and the actual concentration C_r' above a particle. Studies [1, 13] have shown that the growth rates of Si_3N_4 particles do not depend linearly on the concentration gradients. Therefore this assumption is not always true in reality.

4. It is assumed that the mass that dissolves from the subcritical particles precipitates on the large particles without accumulating in the liquid. In reality there is a small accumulation of mass in the liquid medium, and the liquid medium concentration changes with time.
5. Neither Wagner [4] nor Lifshitz and Sloyosov [3] provide sufficient information about the time required for the system to reach the steady-state when the scaled particle size distribution function is independent of time [18, 4].
6. The assumption of isotropic surface energies implies that particle geometries are spherical. As a result, the theory does not describe Ostwald ripening in an anisotropic system of particles such as completely faceted crystals.

The shortcomings discussed above are the reasons why experimentally measured data such as growth exponents, particle size distributions and interfacial reaction rates [13] do not generally agree with the predictions of the LSW theory [5, 18].

3.1.1 Solving the general isotropic problem in the limit of $t \rightarrow \infty$

In the same manner that Wagner [4] studied Ostwald ripening in the two limiting cases of diffusion controlled and interfacial reaction controlled mass transfer, we attempted to solve the problem generally for the isotropic system.

In the limit of $t \rightarrow \infty$, the number of particles that disappear from the system is finite. The distribution function has a finite value as $r \rightarrow 0$ and particles disappear from the system in accordance with eq.(3.3). Considering $r \ll r^*$ in eq.(3.10) yields

$$\dot{r} = - \frac{A k D}{r (kr + D)}, \quad (3.27)$$

where

$$A = \frac{2 \sigma V_m^2 c_o}{RT}.$$

It follows from eq.(3.27) that the distribution function must be proportional to $r(kr + D)$ to ensure that eq.(3.3) has a finite value as $r \rightarrow 0$. Therefore, in the limit of $t \rightarrow \infty$ we assume that the distribution function may be written as the product of a pure function of time and a function of the reduced radius ρ , defined in eq.(3.14):

$$f(r, t) = g(t) r (kr + D) h(\rho).$$

Dividing the left and right hand sides of the equation above by r^* yields an expression in terms of ρ :

$$f(r, t) = g(t) r^* \rho (k r^* \rho + D) h(\rho). \quad (3.28)$$

If eq.(3.28) is substituted into eq.(3.11) it may be shown that the reduced radius distribution function satisfies the condition given by eq.(3.17):

$$r^* = \int_0^\infty g(t) r^* \rho (k r^* \rho + D) h \frac{r^{*3} \rho^2 d\rho}{(k r^* \rho + D)} \bigg/ \int_0^\infty g(t) r^* \rho (k r^* \rho + D) h \frac{r^{*2} \rho d\rho}{(k r^* \rho + D)}.$$

This simplifies to give the condition that $h(\rho)$ must satisfy:

$$\int_0^\infty \rho^2 h(\rho) d\rho = \int_0^\infty \rho^3 h(\rho) d\rho.$$

An expression for $g(t)$ is obtained by substituting eq.(3.28) into eq.(3.4) and eq.(3.14) is used to obtain an expression in terms of ρ :

$$\begin{aligned} \phi &= \int_0^\infty \frac{4\pi}{3} r^{*3} \rho^3 g(t) r^* \rho (k r^* \rho + D) h r^* d\rho \\ &= g(t) \frac{4\pi}{3} r^{*5} \left[r^* \int_0^\infty k \rho^5 h(\rho) d\rho + \int_0^\infty D \rho^4 h(\rho) d\rho \right] \end{aligned}$$

For convenience, the integral expressions above which are independent of time are called α and β respectively, that is

$$\begin{aligned} \alpha &= \int_0^\infty k \rho^5 h(\rho) d\rho \\ \beta &= \int_0^\infty D \rho^4 h(\rho) d\rho, \end{aligned}$$

and $g(t)$ is

$$g(t) = \frac{3\phi}{4\pi} \frac{r^{*-5}(t)}{(r^* \alpha + \beta)}. \quad (3.29)$$

Differentiating eq.(3.29) with respect to time yields

$$\dot{g}(t) = \frac{3\phi}{4\pi} \left[\frac{-5 r^{*-6} \dot{r}^*}{(r^* \alpha + \beta)} \right] + \frac{3\phi}{4\pi} \left[\frac{-\alpha r^{*-5} \dot{r}^*}{(r^* \alpha + \beta)^2} \right] = g(t) \dot{r}^* \left[\frac{-5}{r^*} - \frac{\alpha}{(r^* \alpha + \beta)} \right].$$

Substituting eq.(3.28) into eq.(3.3) and using eq.(3.14) and the above expression to eliminate $g(t)$, an expression for \dot{r}^* may be obtained:

The left hand side of eq.(3.3) is

$$\begin{aligned} \frac{dZ}{dt} &= LHS = \frac{d}{dt} \int_0^\infty f(r, t) dr \\ &= \frac{d}{dt} (g(t)r^{*3}(t)) \int_0^\infty k \rho^2 h d\rho + \frac{d}{dt} (g(t) r^{*2}(t)) \int_0^\infty D \rho h d\rho \\ &= [3 r^{*2} g \dot{r}^* + \dot{g} r^{*3}] \int_0^\infty k \rho^2 h d\rho + [2 r^* g \dot{r}^* + \dot{g} r^{*2}] \int_0^\infty D \rho h d\rho. \end{aligned}$$

Once again for convenience the integrals in the expression above are called δ and ϵ :

$$\begin{aligned} \delta &= \int_0^\infty k \rho^2 h(\rho) d\rho \\ \epsilon &= \int_0^\infty D \rho h(\rho) d\rho, \end{aligned}$$

and using the expression for $\dot{g}(t)$ above to obtain an expression in terms of $g\dot{r}^*$ yields

$$\begin{aligned} LHS &= [3 r^{*2} g \dot{r}^* + \dot{g} r^{*3}] \delta + [2 r^* g \dot{r}^* + \dot{g} r^{*2}] \epsilon \\ &= g\dot{r}^* \left\{ 3 r^{*2} + r^{*3} \left[\frac{-5}{r^*} - \frac{\alpha}{(r^* \alpha + \beta)} \right] \right\} \delta + g\dot{r}^* \left\{ 2 r^* + r^{*2} \left[\frac{-5}{r^*} - \frac{\alpha}{(r^* \alpha + \beta)} \right] \right\} \epsilon. \end{aligned}$$

Substituting eq.(3.27) and eq.(3.28) into the right hand side of eq.(3.3) and using eq.(3.14) yields

$$RHS = \lim_{r=0} (f\dot{r}) = g r^* \rho (k r^* \rho + D) \times \frac{-A k D}{r^* \rho (k r^* \rho + D)} = -A k D g(t).$$

Equating the LHS and RHS of eq.(3.3) yields the expression for \dot{r}^* :

$$\frac{dr^*}{dt} = \frac{-A k D}{\delta \left[-2 r^{*2} - \frac{\alpha r^{*3}}{(r^* \alpha + \beta)} \right] + \epsilon \left[-3 r^* - \frac{\alpha r^{*2}}{(r^* \alpha + \beta)} \right]}. \quad (3.30)$$

It is clear from the expression above that we cannot proceed further with an analytical solution in the manner that Wagner [4] did for the two limiting cases. However, a numerical solution to the problem is possible.

In the diffusion controlled limit ($D \ll kr$) and the interfacial reaction controlled limit ($kr \ll D$) equation (3.30) reduces to the analytical expressions which Wagner [4] obtained.

In the diffusion controlled limit D is set equal to zero in the expressions for integral expressions β and ϵ in eq.(3.30) and substituting the expressions for the constants A and δ into eq.(3.30) yields

$$\begin{aligned} \frac{dr^*}{dt} &= \frac{-2\sigma V_m^2 c_o k D}{-3 r^{*2} RT \int_0^\infty k \rho^2 h(\rho) d\rho} \\ &= \frac{2\sigma c_o V_m^2 D}{3RT \int_0^\infty \rho^2 h(\rho) d\rho} \frac{1}{r^{*2}}. \end{aligned}$$

This expression is the same as the expression for \dot{r}^* obtained analytically by Wagner [4] for the diffusion controlled case.

In the interfacial reaction controlled limit k is set equal to zero in the integral expressions α and δ and substituting the expressions for the constants A and ϵ into eq.(3.30) yields

$$\frac{dr^*}{dt} = \frac{2\sigma c_o V_m^2 k}{3RT \int_0^\infty \rho h(\rho) d\rho} \frac{1}{r^*},$$

which is also the same as the analytical expression obtained by Wagner [4] in this limit.

3.2 Applications of grain growth theories to silicon nitride

Existing theories of Ostwald ripening have led to significant advances in modeling the grain growth behaviour of silicon nitride materials. However, these are also based on isotropic surface energies and growth mechanisms. This means that these models do not take the hexagonal geometry of Si_3N_4 particles into account, nor the fact that the surface energies on the hexagonal and prismatic facets are different. As a result, they do not give a complete description of anisotropic growth of $\beta\text{-Si}_3\text{N}_4$ grains due to the anisotropic growth of the grains in different crystallographic orientations [1].

In a recent study by Kitayama *et al* [5], a thermodynamic model for anisotropic Ostwald ripening of a completely faceted crystal was developed and applied to hexagonal $\beta\text{-Si}_3\text{N}_4$ particles dispersed in a liquid medium. The growth of a hexagonal $\beta\text{-Si}_3\text{N}_4$ particle (refer to fig.(2.3)) is represented by two variables, $a(t)$ and $c(t)$, which represent the width and the length of the particle respectively, at time t . Expressions for the time derivatives of a and c are required to determine how the shape of the particles evolve.

Kitayama *et al* [5] assumed that the driving force for mass transfer is due to a chemical potential difference between the hexagonal and prismatic facets of a $\beta\text{-Si}_3\text{N}_4$ particle and the

surrounding liquid medium. Mass transfer between the facets of a particle is not considered in this model. The chemical potential of a surface depends on the curvature of the surface. Therefore the chemical potential of hexagonal and prismatic facets in terms of the curvature of these facets are

$$\mu_c = \mu_0 + \left(\frac{2 \sigma V_m}{a} \right), \quad (3.31)$$

and

$$\mu_a = \mu_0 + \sigma V_m \left(\frac{1}{a} + \frac{1}{c} \right), \quad (3.32)$$

respectively. μ_0 is the standard chemical potential of an infinitely large surface, σ is the interfacial energy between the particle facets and the liquid medium and V_m is the molar volume of the material. It is clear from the expressions above that Kitayama *et al* assume that the interfacial energies between the two facets and the liquid medium are the same. In reality, the surface energies on the hexagonal and prismatic facets are different (refer to §(2.2.2)).

An imaginary particle of radius r_l which is in equilibrium with the liquid medium is introduced into the model. The chemical potential of the liquid medium may then be expressed in terms of the curvature of this hypothetical particle r_l , that is,

$$\mu_l = \mu_0 + \left(\frac{2 \sigma V_m}{r_l} \right). \quad (3.33)$$

A general expression for the flux J_s of material crossing an interface due to the chemical potential difference between a surface s and the liquid medium is obtained by deriving equations for the flux of material controlled by diffusion and the interfacial reaction processes, and equating

them in equilibrium. This yields

$$J_s = - \frac{1}{k_b T V_m} \frac{D k_s}{D + k_s \Delta s} (\mu_l - \mu_s), \quad (3.34)$$

where k_b is the Boltzmann constant, D is the diffusion constant, k_s is the interfacial reaction constant on a surface s , Δs is the diffusion distance and μ_s is the chemical potential of the surface s .

The flux of material from a surface is related to the change in the dimensions of the surface with time by the expression

$$\frac{ds}{dt} = - J_s \Omega, \quad (3.35)$$

where Ω is defined as the volume of a growth unit [5]. Substituting equations (3.31) to (3.34) into eq.(3.35) yields expressions for the rates at which a and c change with time, that is,

$$\frac{da}{dt} = \frac{\sigma V_m}{RT} \frac{D k_a}{D + k_a a} \left(\frac{2}{r_l} - \frac{1}{a} - \frac{1}{c} \right), \quad (3.36)$$

and

$$\frac{dc}{dt} = \frac{\sigma V_m}{RT} \frac{D k_c}{D + k_c c} \left(\frac{2}{r_l} - \frac{2}{a} \right), \quad (3.37)$$

respectively. The radius r_l corresponding to the concentration in the liquid medium is calculated using the mass conservation law. If there are n particles in the system then index i represents the i^{th} particle. The distance from the centre of the particle to the prismatic facet and the hexagonal facet is a_i and c_i , respectively. Applying the mass conservation law to the system yields

$$\sum_{i=1}^n \left(8 \sqrt{3} a_i c_i \frac{da_i}{dt} + 4 \sqrt{3} a_i^2 \frac{dc_i}{dt} \right) = 0. \quad (3.38)$$

Substituting eq.(3.36) and eq.(3.37) into eq.(3.38) and solving for r_l yields

$$r_l = \frac{\sum_{i=1}^n \left(\frac{2k_a a_i c_i}{D + k_a a_i} + \frac{k_c a_i^2}{D + k_c c_i} \right)}{\sum_{i=1}^n \left(\frac{k_a (a_i + c_i)}{D + k_a a_i} + \frac{k_c a_i}{D + k_c c_i} \right)}. \quad (3.39)$$

The total grain growth during Ostwald ripening is obtained by solving eq.(3.36), eq.(3.37) and eq.(3.39) selfconsistently and numerically [5].

In the computer simulations which Kitayama *et al* [5] performed, a system of 287 particles are generated randomly [5], with the relationship between the length and width of each particle being random. Grain growth simulations are performed to study the effect of the system parameters such as the relationship between the diffusion and interfacial reaction constants on grain growth behaviour of the β -Si₃N₄ particles in the liquid medium. The evolution of aspect ratios of the grains with time are studied and growth exponents are extracted from the model. [5].

Some of the conclusions drawn from this study are listed below:

- Length growth in the β -Si₃N₄ particles is a complex function of time and the relationship between diffusion and interfacial reaction constants.
- For special relationships between the diffusion constants and the interfacial reaction constants, the average aspect ratios in the system obtain constant values after a prolonged time. This implies that the shape of the crystals are determined by kinetics instead of thermodynamics.
- A growth exponent of $n = 3$ is predicted when grain growth is controlled by the interfacial reaction. Higher values for the growth exponents are predicted as the value of the diffu-

sion constant approaches the values of the product of the interfacial reaction constants and the characteristic diffusion distance in the calculations.

Although the work by Kitayama *et al* has led to advances in the understanding of the grain growth of β - Si_3N_4 grains, isotropic surface energies on the hexagonal and prismatic facets are used in the calculations. This model also assumes that mass transfer between the facets of a particle does not occur and eq.(3.38) implies that mass does not accumulate in the liquid medium. They do not use a distribution function to describe the evolution of particles which, for a microscopic sample of material, is more appropriate. Thus this model does not give a complete description of anisotropic Ostwald ripening in Si_3N_4 ceramics.

Chapter 4

Numerical Studies of the Isotropic System

The LSW theory applied to an isotropic system of spherical particles was studied numerically in order to determine the numerical methods necessary for a stable solution to the anisotropic problem.

Wagner [4] derived a general theory to describe Ostwald ripening in a system of spherical particles and then obtained analytical solutions to the problem in the two limiting cases of diffusion controlled and interfacial reaction controlled mass transfer in the steady state.

Numerical solutions for the two limiting cases and the general case were obtained. The numerical methodology is described below.

4.1 Numerical solution to the isotropic problem in the diffusion and interfacial reaction controlled limits

The methodology used to obtain numerical solutions to the diffusion and interfacial reaction controlled limits are identical. Therefore the numerical methods applied to only the diffusion controlled case is described below.

A numerical solution to the diffusion controlled case was obtained by numerically integrating the ordinary differential equation (3.23) in order to determine a form for the reduced radius distribution function $h(\rho)$. The fourth order Runge-Kutta method [19] for integrating ordinary differential equations was used to achieve this, and the numerical results were compared to the analytical solutions (eq.(3.24)) obtained by Wagner [4].

The diffusion controlled case may be classed as an initial value problem where

$$h(\rho = 0) = 1. \quad (4.1)$$

The fourth order Runge-Kutta method [19] was used to integrate a discrete version of the ordinary differential equation (3.23)

$$\left. \frac{dh}{d\rho} \right|_i = \frac{(3 - 6\gamma^{-1}\rho_i^2)}{(\gamma^{-1}\rho_i^3 - 3\rho_i + 3)} h_i = g(\rho_i, h_i) \quad (4.2)$$

in order to calculate h . The index i represents discrete points in space and h_i represents the value of the reduced radius distribution function at discrete points ρ_i in space, that is,

$$\rho_i = i \Delta\rho \quad i = 0, 1, 2, \dots, I,$$

and

$$h_i = h(\rho_i). \quad (4.3)$$

The Runge-Kutta method evaluates the slope at four points in the interval i to $i + 1$, namely at the end points (i and $i + 1$) and at two estimated midpoints in the interval [19], that is,

$$\begin{aligned} k_1 &= g(\rho_i, h_i) \\ k_2 &= g\left(\rho_i + \frac{\Delta\rho}{2}, h_i + k_1/2\right) \\ k_3 &= g\left(\rho_i + \frac{\Delta\rho}{2}, h_i + k_2/2\right) \\ k_4 &= g(\rho_i + \Delta\rho, h_i + k_3), \end{aligned} \quad (4.4)$$

and h_{i+1} is calculated by the expression [19]

$$h_{i+1} = h_i + \frac{\Delta\rho}{6} (k_1 + 2k_2 + 2k_3 + k_4). \quad (4.5)$$

The evolution of the function $h(\rho)$ and the value of the parameter γ are calculated in a self-consistent manner described below:

In the calculation, the parameter γ is given an arbitrary initial value, h_{i+1} is calculated at the points in the range $i = 0$ to $i = I - 1$ and a new value for γ is calculated by numerically integrating eq.(3.20) using Simpson's rule (eq.(4.16)). The new value of γ is then used to recalculate h , and a new value for γ is also recalculated. This cyclic calculation of h and γ is repeated until selfconsistency is achieved.

Structure of the calculation for the diffusion controlled case

1. Define all constants and variables.
2. Repeat the following cycle until selfconsistency is achieved:
 - $h(0) = 1$.
 - For $i = 0$ to $i = I - 1$ calculate h_{i+1} using eq.(4.5).
 - Calculate a new value for γ using eq.(3.20) and Simpson's rule.
 - if the difference between the previous value of γ and the new value is less than 10^{-6} :
 - write data to a file,
 - stop the cycle.
 - Otherwise use the new value of γ , and
 - repeat the calculation.
3. Stop.

4.2 Numerical solution of the general isotropic problem

The general isotropic problem may be classed as a one dimensional flux-conservative problem. The change in the spherical particle size distribution function $f(r, t)$ [4] with time is obtained by differentiating a discrete version of the isotropic continuity equation (3.5). The Two-Step Lax-Wendroff finite differencing method is used to achieve this.

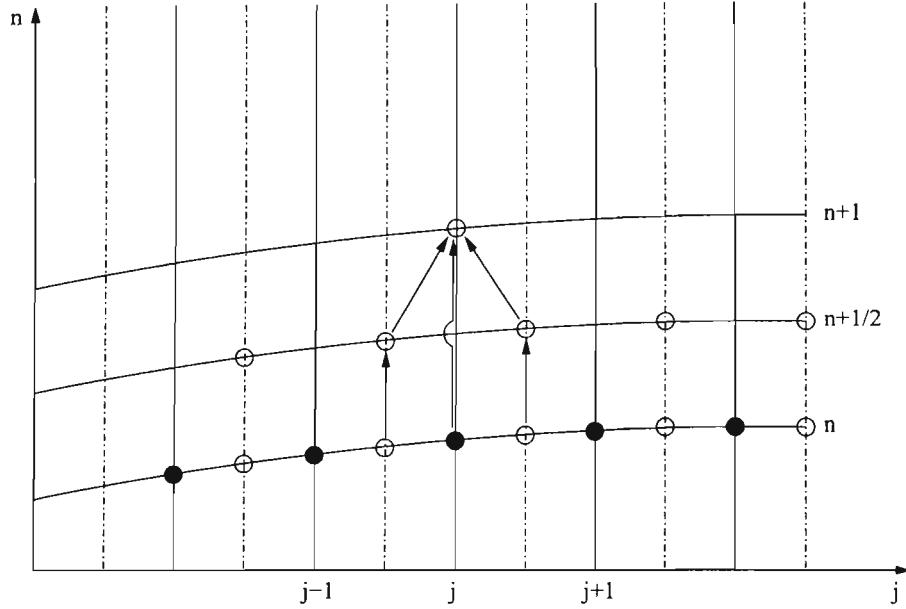


Figure 4.1: Schematic representation of the two step Lax-Wendroff differencing method. The solid dots represent the initial values of the distribution function. These are used to calculate the values at the half space and half time step, represented by the unfilled circles, and are then used to calculate the value of the distribution function at the next full time step.

It is referred to as a two-step method since the intermediate quantities $f_{j+1/2}^{n+1/2}$ are calculated at the half space steps $r_{j+1/2}$ and the half time steps $t_{n+1/2}$, which are then used to calculate f_j^{n+1} , the value of the distribution function at the next time step (refer to fig.(4.1)). This method is second-order in time and space [19], that is, the errors are second order in Δt and in Δr . The subscripts j and n are used to represent discrete points in space and time respectively, and $f(r_j, t_n)$ is represented by f_j^n . The numerical scheme used to calculate the quantities $f_{j+1/2}^{n+1/2}$ and f_j^{n+1} was adopted from reference [20].

The finite-difference representation of the left and right hand side of equation (3.5) at an

intermediate point $(j + 1/2, n)$ is

$$\frac{f_{j+1/2}^{n+1/2} - f_{j+1/2}^n}{\left(\frac{\Delta t}{2}\right)} = -\frac{1}{\Delta r} (f_{j+1}^n \dot{r}_{j+1}^n - f_j^n \dot{r}_j^n). \quad (4.6)$$

Solving for $f_{j+1/2}^{n+1/2}$ yields

$$f_{j+1/2}^{n+1/2} = f_{j+1/2}^n - \frac{\Delta t}{2\Delta r} (f_{j+1}^n \dot{r}_{j+1}^n - f_j^n \dot{r}_j^n). \quad (4.7)$$

The direction of the flux of particles $f\dot{r}$ at the point $(j + 1/2, n)$ is used to determine $f_{j+1/2}^n$. If the direction of the flux is to the right, that is, $\dot{r}_{j+1/2} > 0$ let

$$\begin{aligned} d_1 &= f_j^n + \frac{1}{2} (f_j^n - f_{j-1}^n) \\ d_2 &= \frac{1}{2} (f_j^n + f_{j+1}^n) \\ d_3 &= f_j^n, \end{aligned} \quad (4.8)$$

then

$$f_{j+1/2}^n = \begin{cases} \max [d_3, \min(d_1, d_2)] & \text{if } f_j^n \leq f_{j+1}^n \\ \min [d_3, \max(d_1, d_2)] & \text{if } f_j^n \geq f_{j+1}^n. \end{cases} \quad (4.9)$$

In (4.8) d_1 is obtained by interpolating between f_j^n and f_{j-1}^n and d_2 is the average of f_j^n and f_{j+1}^n .

Similarly if $\dot{r}_{j+1/2} < 0$ let

$$\begin{aligned} d_1 &= f_{j+1}^n + \frac{1}{2} (f_{j+1}^n - f_{j+2}^n) \\ d_2 &= \frac{1}{2} (f_j^n + f_{j+1}^n) \\ d_3 &= f_{j+1}^n \end{aligned} \quad (4.10)$$

then

$$f_{j+1/2}^n = \begin{cases} \max [d_3, \min(d_1, d_2)] & \text{if } f_j^n \leq f_{j+1}^n \\ \min [d_3, \max(d_1, d_2)] & \text{if } f_j^n \geq f_{j+1}^n. \end{cases} \quad (4.11)$$

Calculating $f_{j+1/2}^n$ in this manner ensures that its value is bounded between 0 and the lowest positive value which guarantees a smooth well behaved function.

Similarly the equation corresponding to (4.7) for the point $(j - 1/2, n)$ is obtained, the fluxes $f_{j\pm 1/2}^{n\pm 1/2} \dot{r}_{j\pm 1/2}$ are calculated and f_j^{n+1} is obtained by the properly centred expression [19],

$$f_j^{n+1} = f_j^n - \frac{\Delta t}{\Delta r} \left(f_{j+1/2}^{n+1/2} \dot{r}_{j+1/2}^{n+1/2} - f_{j-1/2}^{n+1/2} \dot{r}_{j-1/2}^{n+1/2} \right). \quad (4.12)$$

If the calculation produces negative values for f_j^{n+1} an interpolation is carried out to correct this. The furthest point j from the origin at which f_j^{n+1} has a negative value is determined and from $j = 0$ to that point the values for f_j^{n+1} are recalculated using eq.(3.28). The discrete version of eq.(3.28) is

$$f(r_j, t_n) = r_j (k r_j + D). \quad (4.13)$$

Equation (3.28) was chosen as the interpolating function which is the small- r Taylor-expanded version of f close to the origin. This interpolation ensures that the distribution function remains positive, and that the flux at the origin, namely $f\dot{r}$ attains a finite value in the steady state.

A stable solution to the problem requires that the time step used in the calculations must be neither too large nor too small. According to the von Neumann stability analysis [19] of the Lax-Wendroff method, the time step is required to satisfy the condition that

$$\Delta t \leq \left| \frac{\Delta r}{\dot{r}_j} \right| \quad j = \frac{1}{2}, 1, \frac{3}{2}, 2, \dots, J. \quad (4.14)$$

Reference [20] found that a time step given by

$$\Delta t = 0.8 \left| \frac{\Delta r}{\dot{r}_{1/2}} \right|, \quad (4.15)$$

produced stable solutions for the numerical solution of island coarsening on thin films which was described by the LSW theory [3, 4]. Consequently, this expression for Δt was adopted and used in the calculations for the isotropic system.

The change in the total number of particles in the system, the total volume of solid particles (refer §(2.3.1) for the expressions) and the volume per particle as a function of time are calculated by numerical integration using Simpson's rule

$$\int_a^b f(r_j) dr \approx \frac{\Delta r}{3} \left[f(a) + 2 \sum_{j=1}^{J-1} f(r_{2j}) + 4 \sum_{j=1}^J f(r_{2j-1}) + f(b) \right]. \quad (4.16)$$

The initial distribution function may be described by a Gaussian, logarithmic, log-normal or bimodal expression. It is represented by its value at a discrete number of equally spaced points, that is,

$$f(r, t) \rightarrow f(r_j, t_n), \quad (4.17)$$

where

$$r_j = j \Delta r \quad j = 0, 1, 2, \dots, J, \quad (4.18)$$

and

$$t_n = n \Delta t \quad n = 0, 1, 2, \dots, N. \quad (4.19)$$

The growth exponents n are obtained by plotting $(\text{volume}/\text{particle})^{\frac{n}{3}}$ versus time for different values of the diffusion constant D , where $n = 1, 2, 3, 4, 5$. The value of n and D which yield

linear relationships represents the value of the growth exponent and the mechanism of grain growth, respectively.

Basic structure of the calculation

1. Declare all constants and variables.

2. At $t = 0$:

- Generate the initial distribution function $f(r_j, 0)$ and normalise it using eq.(4.16).
- Calculate:
 - the total volume of solid using eq.(3.4)
 - the critical radius r^* using eq.(3.11),
 - $\dot{r}_{1/2}$
 - the time step Δt using (4.15).

3. Loop over time:

- Calculate
 - $\dot{r}_{j+1/2}$
 - $f_{j+1/2}^n$ using equations (4.9) and (4.11))
 - $f_{j+1/2}^{n+1/2}$ using eq.(4.7)
 - r^* at $n + 1/2$
 - f_j^{n+1} using eq.(4.12)
 - * If f_j^{n+1} is negative interpolate to the origin:

- find r_j for which f_j^{n+1} is negative,
 - for $j = 0$ to j recalculate f_j^{n+1} using eq.(4.13).
- the total volume, and
 - the total number of particles in the system.
- Write out data to files.

4. Stop.

4.3 Results and discussion

4.3.1 Numerical solution to the diffusion and interfacial reaction controlled limits of mass transfer

The diffusion controlled and the interfacial reaction controlled limits of the LSW theory [3, 4] were studied numerically. The values for the parameter γ and the final form of the reduced radius distribution function $h(\rho)$ were determined and compared with the analytical results that Wagner [4] obtained in his study of these two special cases.

Diffusion controlled mass transfer

The numerical solution to the problem in the diffusion controlled limit yielded a value of 2.2499 for the parameter γ . The form of the reduced radius distribution function $h(\rho)$ that was obtained numerically is presented below:

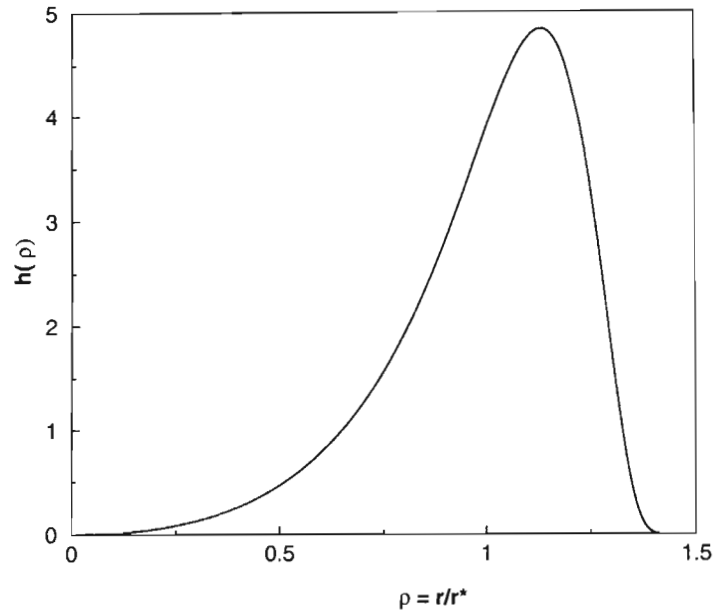


Figure 4.2: The reduced radius distribution function in the diffusion controlled limit obtained numerically. The value of the parameter γ was calculated to be 2.2499.

Wagner obtained a value of $9/4$ for the parameter γ [4] and the analytical expression eq.(3.24) for the distribution function $h(\rho)$ which was plotted and is presented below:

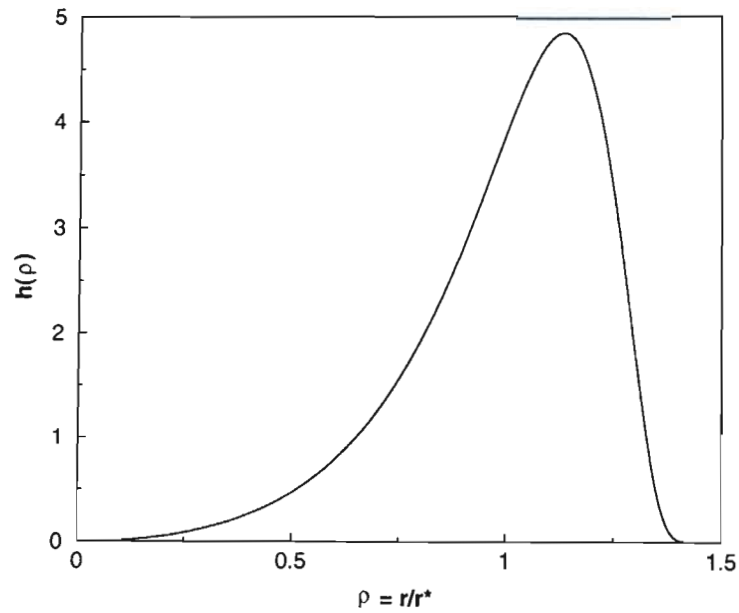


Figure 4.3: The reduced radius distribution function obtained analytically by Wagner [4] for diffusion controlled mass transfer. The value of the parameter γ was $9/4$.

The numerical solution of the problem in the diffusion controlled case is in excellent agreement with the analytical solution obtained by Wagner [4].

Interfacial reaction controlled mass transfer

The numerical solution of the interfacial reaction controlled limit yielded a value of 1.3334 for the parameter γ . The reduced radius distribution function that was calculated is presented below:

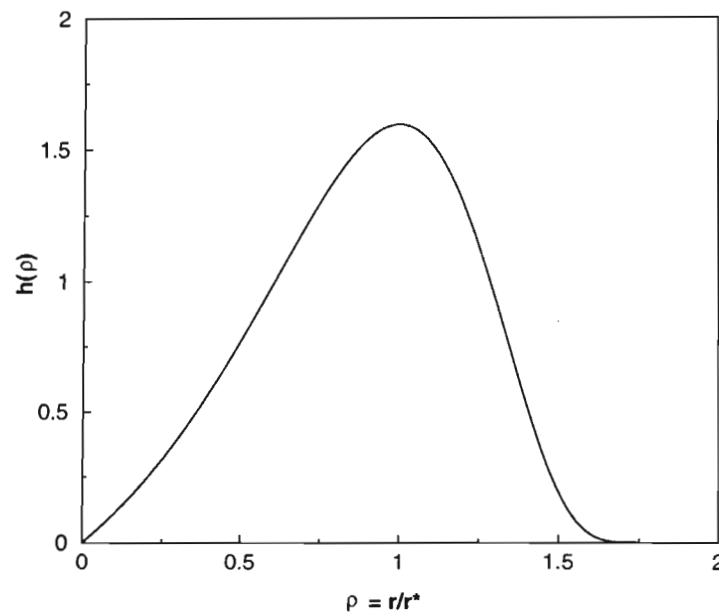


Figure 4.4: The reduced radius distribution function obtained numerically corresponding to a value of 1.3334 for the parameter γ in the interfacial reaction controlled limit.

These numerical solutions compare excellently with the results obtained by Wagner in this limit [4], which are presented below:

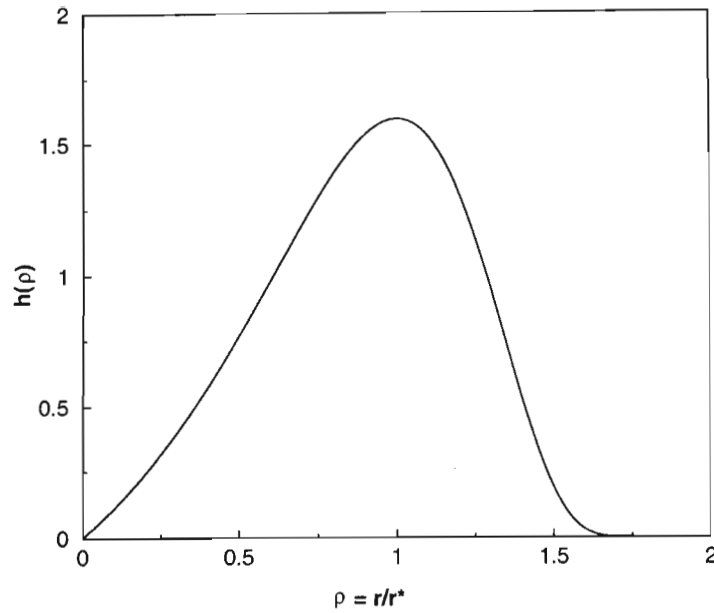


Figure 4.5: The reduced radius distribution function obtained analytically by Wagner [4] in the interfacial reaction controlled limit. A value of $4/3$ was obtained for the parameter γ .

Once again the agreement between the analytical and the numerical solutions is excellent. The numerical solutions were obtained by solving eq.(3.23) (and the corresponding equation for the interfacial reaction controlled limit) without making further approximations. After deriving eq.(3.23) (and the corresponding equation for the interfacial reaction controlled limit) Wagner [4] made further approximations to obtain the analytical solutions. Therefore the agreement between the numerical and the analytical solutions implies that the approximations made by Wagner are justified.

4.3.2 Numerical solution to the general isotropic problem

The isotropic system was studied numerically in a great deal of detail to develop the numerical methods necessary for a stable solution to the anisotropic problem. However numerical

instabilities associated with the $1/r$ term as $r \rightarrow 0$ in eq.(3.10) arose in the calculations and at present we are still trying to cope with these numerical instabilities. As a result, we are only able to present some preliminary results from the calculations carried out to date.

Data used for modeling

Our best estimates to date of the values for the fundamental parameters such as the interfacial energies, diffusion and interfacial reaction constants and saturation concentrations for a system of isotropic Si_3N_4 particles are listed in the table below:

Sintering temperature:	2123 K
Diffusion constant:	$D_o = 10^4 \text{ m}^2\text{s}^{-1}$, $Q = -545 \text{ kJ mol}^{-1}$ $D = D_o \exp (Q/RT)$
Reaction constant:	$k_{100} = 9.9 \times 10^{-9} \text{ ms}^{-1}$
Interfacial energy:	$\sigma_{100} = 0.10 \text{ Jm}^{-2}$
Saturation:	$C_{100}^o = 1.3 \times 10^4 \text{ mol m}^{-3}$

Table 4.1: A table of the values of the fundamental parameters of Si_3N_4 used in the numerical study of the isotropic system.

The values for the surface energies and diffusion and interfacial reaction constants used in our calculations were selected from data used by Kitayama *et al* [5] and Herrmann [1]. The values for the interfacial energy and the interfacial reaction constant associated with the prismatic (100) facet of a Si_3N_4 crystal were used in the calculations.

Evolution of the distribution function

The initial distribution function was chosen to be a Gaussian function of the form

$$f(r_j, t = 0) = \exp \left[-\frac{1}{2} \left(\frac{r_j - r_o}{\Delta} \right)^2 \right].$$

The value for the constant r_o , which is the radius at which $f(r, t = 0)$ has a maximum value, was chosen to be $5.0 \mu\text{m}$. The value of the constant Δ which represents the spread in the particle radii was chosen to be $1 \mu\text{m}$. Comparing the values for D and kr_o indicated that $kr_o \ll D$. Therefore mass transfer in this calculation is controlled by the interfacial reaction.

The evolution of the distribution function was obtained using the Lax-Wendroff two-step method described in §(4.2):

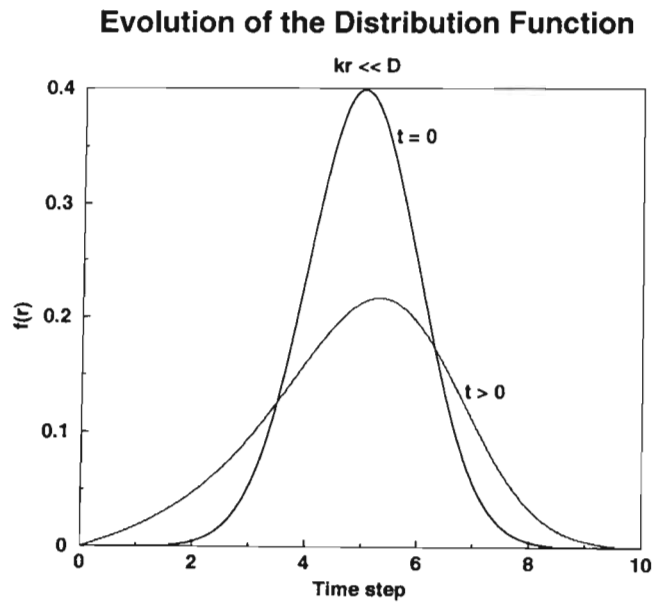


Figure 4.6: Evolution of the distribution function with time.

In fig.(4.6) above, the final distribution function achieves the form predicted by Wagner in the reaction controlled limit with the characteristic linear dependence on r close to the origin.

Change in the number of particles with time

The number of particles as a function of time appears in the figure below:

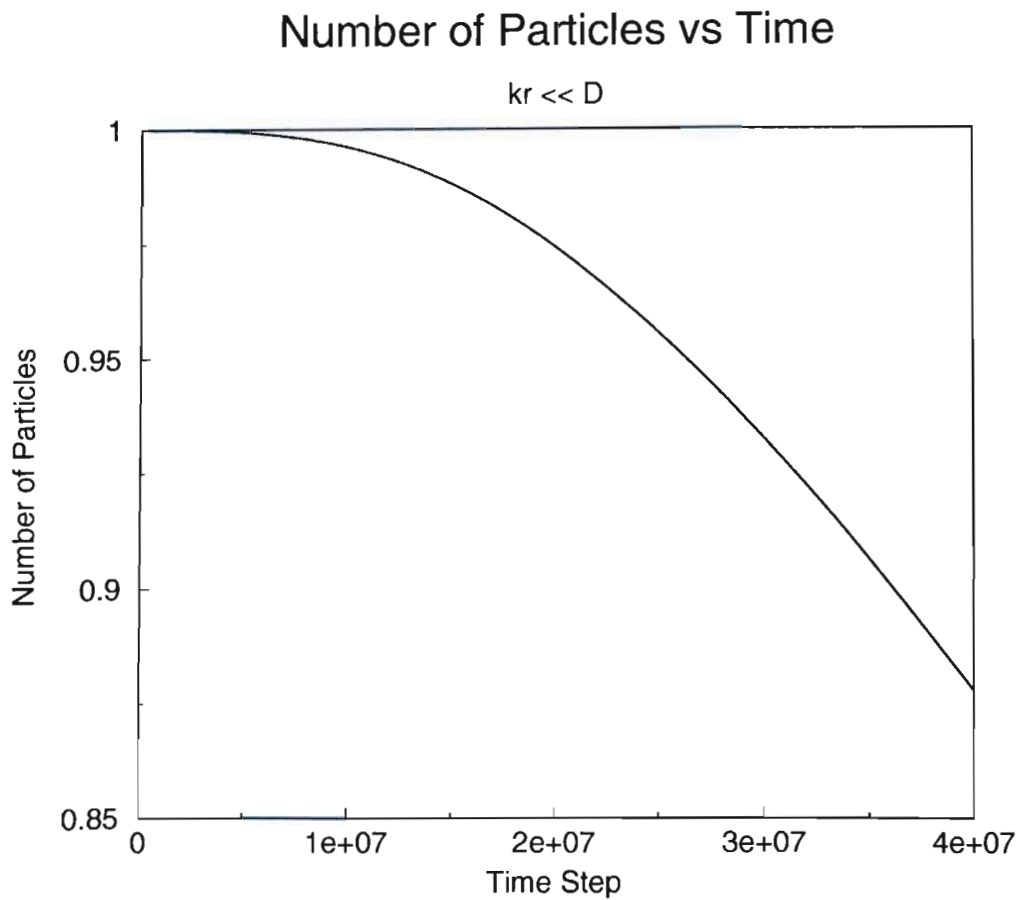


Figure 4.7: Change in the number of particles as a function of time.

The number of particles in the system decreases with time. This is expected since the particles in the system grow by Ostwald ripening.

Change in the total volume with time

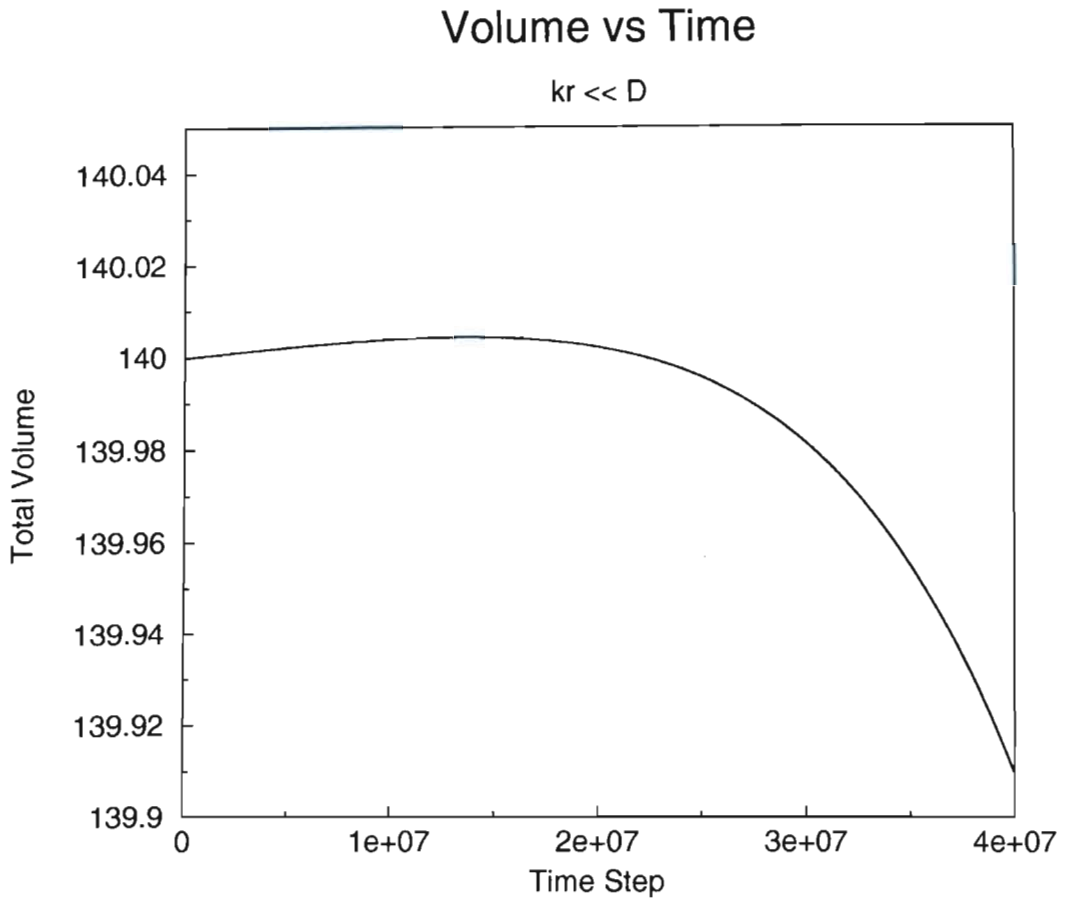


Figure 4.8: Change in the total volume of solid particles in the system as a function of time.

The total volume of solid in the system decreases as a function of time. This means that mass is not conserved as is assumed in the LSW theory. Instead, mass accumulates in the liquid medium, although this accumulation is small.

The volume per particle as a function of time is presented below:

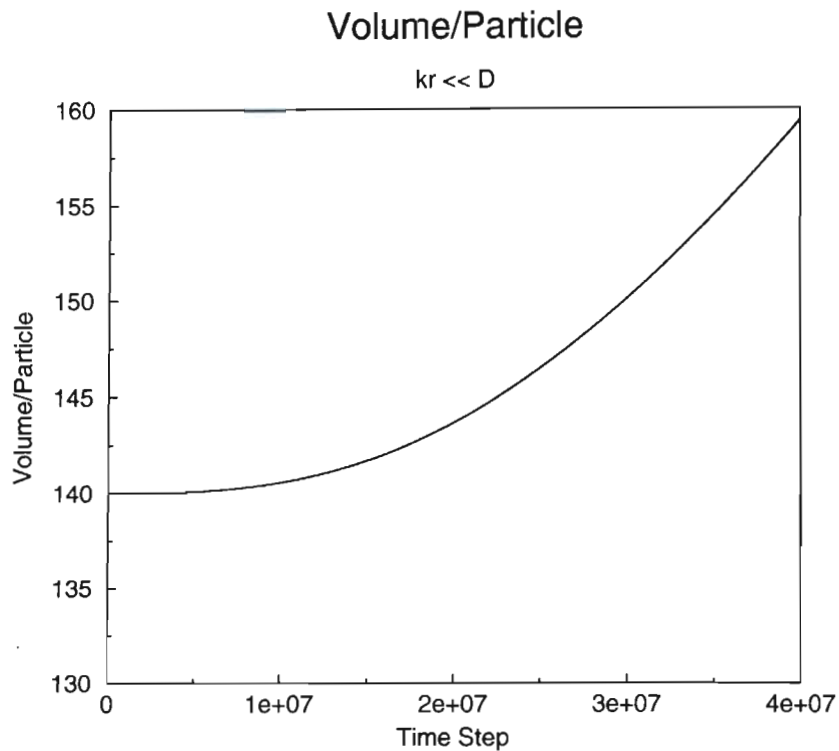


Figure 4.9: Volume per particle as a function of time.

As expected, the volume per particle increases as a function of time since the average size of the particles increases with time by Ostwald ripening.

Extraction of growth exponents

Growth exponents n were obtained by plotting $(volume/particle)^{n/3}$ for various values of n .

The results are presented below:

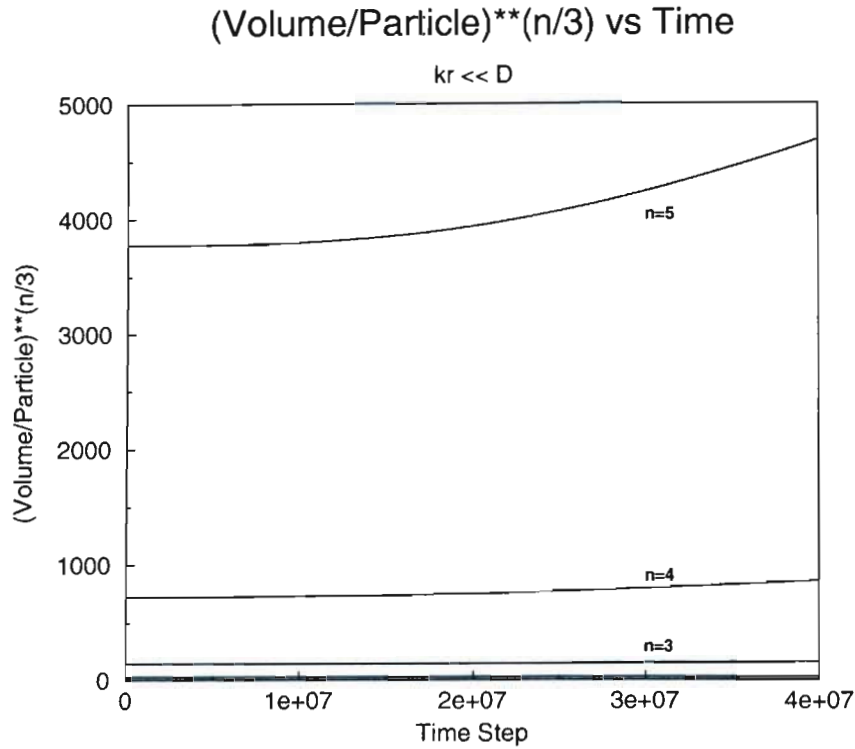


Figure 4.10: Growth exponents obtained from plotting $(volume/particle)^{n/3}$ vs time for $n = 1, 2, 3, 4, 5$.

Since these are preliminary results, no conclusions about the mechanism of grain growth may be drawn as yet. This is the subject of on-going work, and will be the basis of a PhD study.

The use of lower values for D_o in calculations resulted in singularities at the origin due to the $1/r$ term in eq.(3.10). This has hampered further investigations of the isotropic system at present. We are trying to understand these numerical instabilities in order to overcome them so that we may continue with the study of the isotropic system as the basis of an eventual complete numerical analysis of the anisotropic system.

Chapter 5

Anisotropic Coarsening Theory

5.1 Formulation of the anisotropic coarsening theory

The anisotropic coarsening theory (ACT) is a generalisation of the formulation of the LSW theory by Wagner [4]. It describes grain growth in a system of anisotropic particles such as completely faceted crystals. It is based on a diffusion process, and the basic equations of the model have to be solved selfconsistently in order to describe the grain growth behaviour of the anisotropic system of particles surrounded by a second medium. In this thesis, the case example of the anisotropic coarsening of hexagonal Si_3N_4 is investigated.

The ACT is a general theory applicable to anisotropic systems such as silicon nitride and other faceted crystals. The motivation for applying the ACT is that the liquid is assumed to have good wettability so that all particles in the system are completely surrounded by the liquid medium and the liquid fills all the pores in the system completely. Consequently, pore dynamics may be ignored. Neck formation between particles does not occur since the particles

grow by Ostwald ripening. This also allows for grain boundary dynamics to be ignored. The grains are assumed to be essentially independent and only interact with each other via the surrounding liquid medium.

A silicon nitride particle may be viewed as a tiny hexagonal prism. Half the distance between opposite prismatic facets is called the lateral radius a and half the distance between the hexagonal facets is called the longitudinal radius c .

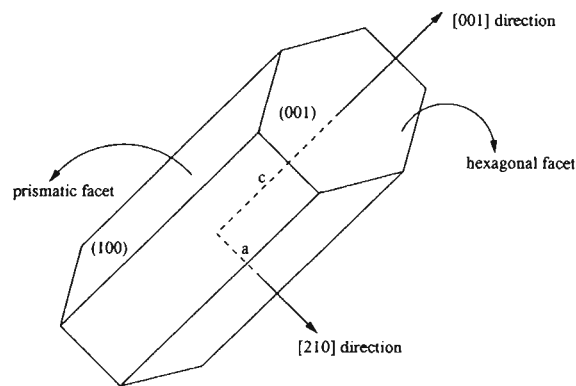


Figure 5.1: Diagram of a hexagonal β -Si₃N₄ particle illustrating the hexagonal and prismatic facets, and the lateral radius a and the longitudinal radius c .

The volume of a hexagonal crystal is

$$V = 4\sqrt{3} a^2 c. \quad (5.1)$$

The surface area of the hexagonal and prismatic facets are

$$A_{001} = 2\sqrt{3} a^2 \quad (5.2)$$

and

$$A_{100} = \frac{4}{\sqrt{3}} ac, \quad (5.3)$$

respectively.

A prism grows epitaxially by adding layers of Si_3N_4 either along the (001) or along the (100) direction. The energy per atom required to add a layer of atoms onto a surface is defined to be the chemical potential of that surface. The expressions for the chemical potential of the hexagonal and the prismatic facets are derived below.

A layer of Si_3N_4 of thickness dc added along the (001) direction corresponds to a change in c . The change in the volume of the crystal due to the change in c is

$$(dV)_a = 4\sqrt{3} a^2 dc. \quad (5.4)$$

The number of moles of Si_3N_4 in a hexagonal prism having volume V , given by eq.(5.1), is

$$n = \frac{V}{V_m}, \quad (5.5)$$

where V_m is the molar volume of the material. Therefore, the corresponding change in the number of moles due to a change in c is

$$(dn)_a = \frac{(dV)_a}{V_m} = \frac{4\sqrt{3} a^2 dc}{V_m}. \quad (5.6)$$

Similarly, adding a layer of material of thickness da along the (100) direction corresponds to a change in a , and the corresponding equations for the change in the volume and number of moles are

$$(dV)_c = 8\sqrt{3} ac da, \quad (5.7)$$

and

$$(dn)_c = \frac{(dV)_c}{V_m} = \frac{8\sqrt{3} ac dc}{V_m}, \quad (5.8)$$

respectively.

The total surface energy E of a particle is

$$E = 2 \times 4\sqrt{3} a^2 \sigma_{001} + 6 \times 8\sqrt{3} ac \sigma_{100}, \quad (5.9)$$

where σ_{001} and σ_{100} are the surface energies of the hexagonal and the prismatic facets, respectively. When the particles are in contact with a liquid medium, as is the case during liquid phase sintering, the surface energy is in reality the interfacial energy between the surface and the liquid medium.

The change in surface energy of the single hexagonal facet due to a change in c and a is

$$(dE)_a = \sigma_{100} 8\sqrt{3} ac dc, \quad (5.10)$$

and that for the single prismatic facet is

$$(dE)_c = \sigma_{001} 8\sqrt{3} a da + \sigma_{100} 8\sqrt{3} c da. \quad (5.11)$$

From the expressions derived above, it follows that the chemical potential of the hexagonal and the prismatic facets are given by

$$\mu_{001} = \left(\frac{dE}{dn} \right)_a = \frac{2\sigma_{100}V_m}{a}, \quad (5.12)$$

and

$$\mu_{100} = \left(\frac{dE}{dn} \right)_c = V_m \left(\frac{\sigma_{001}}{c} + \frac{\sigma_{100}}{a} \right), \quad (5.13)$$

respectively.

During liquid-phase sintering, the system tries to achieve its lowest possible free energy. The particles reduce their overall surface area as a means of achieving this. It is clear that smaller particles have a higher chemical potential and will shrink in size, while larger particles which have a lower chemical potential will grow in size at the expense of the smaller particles. This phenomenon is known as Ostwald ripening.

Since the ACT is based on a diffusion process, it is necessary to find expressions for the concentrations above the hexagonal and prismatic facets. The expressions for the ideal concentrations are derived below.

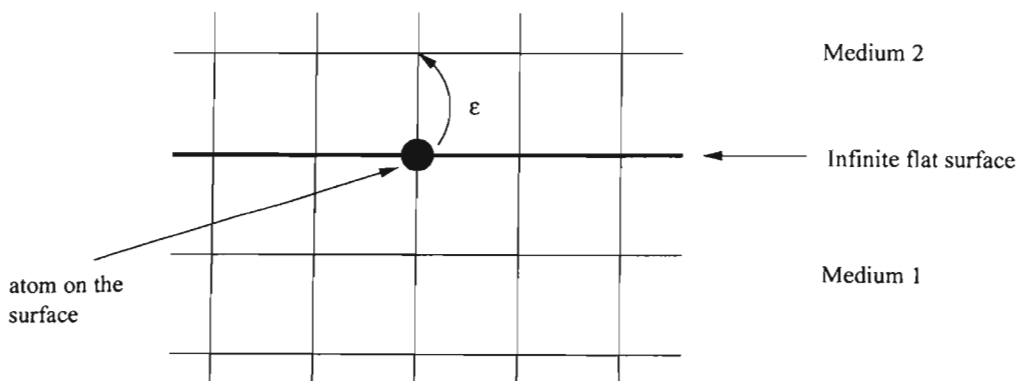


Figure 5.2: Illustration of an atom on an infinite flat surface. The energy required to create a vacancy on the surface is ϵ .

As illustrated in fig.(5.2), the movement of an atom from an infinite flat surface into the second medium results in the creation of a vacancy on the surface. The surface is assumed to be a few atomic layers thick. The chemical potential of an infinite flat surface is zero and the energy required to create a vacancy is ϵ . For convenience, a lattice is used to represent the position of atoms on the infinite flat surface. If there are N_s lattice sites then the number of vacancies in equilibrium at temperature T is

$$n(T) = N_s \frac{e^{-\epsilon/RT}}{1 + e^{-\epsilon/RT}} \approx N_s e^{-\epsilon/RT},$$

where $\epsilon \gg RT$. It follows that the concentration above the surface will be obtained by dividing the expression above by the molar volume of material in medium 2, that is,

$$C_s(T) \approx \frac{N_s}{V_2} e^{-\epsilon/RT}.$$

A surface with a positive radius of curvature has a higher chemical potential than an infinite flat surface.

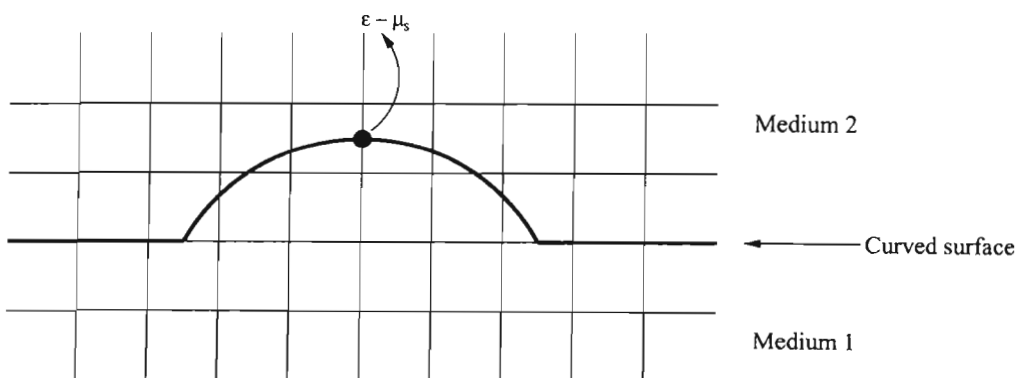


Figure 5.3: Illustration of an atom on a curved surface. The energy required to create a vacancy on the surface is $\epsilon - \mu_s$.

Therefore, the atoms on the surface will have a higher energy due to the curvature of the surface and, as a result, the energy required to create a vacancy on a curved surface will be lower compared to that for a flat surface. If μ_s is the chemical potential of the curved surface, it follows that the energy required to create a vacancy is $(\epsilon - \mu_s)$. Replacing ϵ in the expressions above by $(\epsilon - \mu_s)$ yields the number of vacancies on the curved surface in equilibrium at temperature T :

$$n(T) \approx N_s e^{- (\epsilon - \mu_s) / RT}.$$

The number of vacancies on the surface is equal to the number of atoms above the surface. Dividing the expression above by the molar volume in medium 2 yields the equilibrium concentration above the surface:

$$C_s(T) = \frac{N_s}{V_2} e^{- (\epsilon - \mu_s) / RT} \rightarrow C_s^o e^{\mu_s / RT}.$$

$C_s^o = (N_s/V_2) e^{- \epsilon / RT}$ is the saturation concentration above an infinite flat surface.

In liquid-phase sintering, medium 1 consists of the solid particles and medium 2 is the liquid medium which surrounds the particles.

The equilibrium concentration above a surface is that concentration for which the surface energy of the crystal is a minimum [4], and for which the surface is in equilibrium with the liquid medium. It is also referred to as the ideal concentration above the surface. Substituting the expressions for the chemical potentials above the hexagonal (eq.(5.12)) and prismatic facets (eq.(5.13)) for μ_s into the expression above yields expressions for the equilibrium concentrations

above the respective facets:

$$C_{001} = C_{001}^o \exp \left[\frac{2 \sigma_{100} V_m}{aRT} \right], \quad (5.14)$$

and

$$C_{100} = C_{100}^o \exp \left[\frac{V_m}{RT} \left(\frac{\sigma_{100}}{a} + \frac{\sigma_{001}}{c} \right) \right]. \quad (5.15)$$

C_{001}^o and C_{100}^o are the saturation concentrations above the corresponding infinite large surfaces and V_m is the molar volume of Si_3N_4 . In general, the exponent is very much less than 1 [4]. Therefore the Taylor expansion may be applied to equations (5.14) and (5.15) giving the following approximate expressions:

$$C_{001} = C_{001}^o \left[1 + \frac{2 \sigma_{100} V_m}{aRT} \right], \quad (5.16)$$

and

$$C_{100} = C_{100}^o \left[1 + \frac{V_m}{RT} \left(\frac{\sigma_{100}}{a} + \frac{\sigma_{001}}{c} \right) \right]. \quad (5.17)$$

The system of hexagonal Si_3N_4 particles is described in terms of a distribution function which is defined as

$$f(a, c, t) = \lim_{\substack{\Delta a \rightarrow 0 \\ \Delta c \rightarrow 0}} \frac{N(a, a + \Delta a, c, c + \Delta c, t)}{\Delta a \Delta c}, \quad (5.18)$$

where $N(a, a + \Delta a, c, c + \Delta c, t)$ is the number of particles with lateral radius in the range a to $a + \Delta a$ and longitudinal radius in the range c to $c + \Delta c$ at an instant t in time.

It is assumed that the system consists of a dilute dispersion of particles, which means that the interparticle distance is larger than the largest dimension of a particle. The particles in the system either grow or shrink by Ostwald ripening. The change in the number of particles with lateral radius in the range a to $a + da$ and longitudinal radius in the range c to $c + dc$ is obtained as follows:

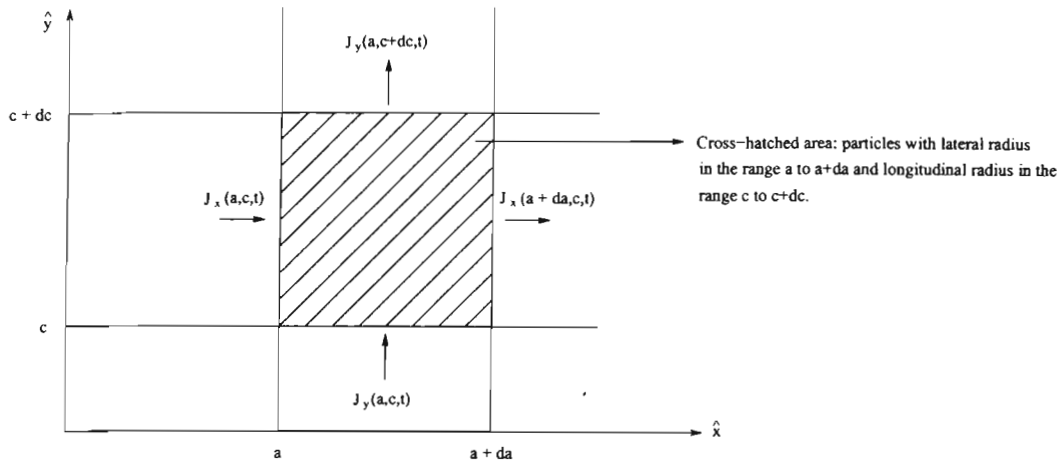


Figure 5.4: Diagram illustrating the change in the number of particles within the cross-hatched region.

[A] It follows from the eq.(5.18) that the number of particles in the cross-hatched area at time t is

$$dN(t) = f(a, c, t) da dc.$$

At a later time $t + dt$ the number of particles in the cross-hatched area is

$$\begin{aligned} dN(t + dt) &= f(a, c, t + dt) da dc \\ &\approx \left[f(a, c, t) + \frac{\partial f}{\partial t} dt \right] da dc. \end{aligned}$$

Therefore, the change in the number of particles in the cross-hatched area when $t \rightarrow t + dt$ is

$$\frac{\partial f}{\partial t} dt da dc.$$

[B] The flux of particles at a point (a, c) at time t in the \hat{x} and the \hat{y} directions is given by

$$J_x(a, c, t) = \frac{f(a, c, t) da dc}{dc dt} = f(a, c, t) \dot{a},$$

and

$$J_y(a, c, t) = \frac{f(a, c, t) da dc}{da dt} = f(a, c, t) \dot{c},$$

respectively. \dot{a} and \dot{c} are the rates at which the lateral and longitudinal radii change with time.

The change in the number of particles in the cross-hatched area when $t \rightarrow t + dt$ is therefore given by

$$\begin{aligned} & [J_x(a, c, t) - J_x(a + da, c, t)] dc dt + [J_y(a, c, t) - J_y(a, c + dc, t)] da dt \\ &= - \frac{\partial J_x(a, c, t)}{\partial a} da dc dt - \frac{\partial J_y(a, c, t)}{\partial c} dc da dt \\ &= - \frac{\partial}{\partial a} (f(a, c, t) \dot{a}) da dc dt - \frac{\partial}{\partial c} (f(a, c, t) \dot{c}) dc da dt. \end{aligned}$$

It follows from [A] and [B] above that

$$\frac{\partial f}{\partial t} = - \frac{\partial}{\partial a} (f \dot{a}) - \frac{\partial}{\partial c} (f \dot{c}). \quad (5.19)$$

Equation (5.19) is a continuity equation and it is the rate at which the distribution function changes with time.

The total number of particles in the system, from the definition of eq.(5.18), is

$$N = \int_0^\infty f(a, c, t) \, dadc. \quad (5.20)$$

The number of particles within a area element $dadc$ is

$$dN = f(a, c, t) \, dadc.$$

The change in the total number of particles with time is

$$\begin{aligned} \frac{dN}{dt} &= \frac{d}{dt} \int_0^\infty f(a, c, t) \, dadc \\ &= \int_0^\infty \frac{\partial f(a, c, t)}{\partial t} \, dadc. \end{aligned}$$

Using the continuity equation (5.19) in the expression above:

$$\begin{aligned} \frac{dN}{dt} &= - \int_0^\infty \left[\frac{\partial(f\dot{a})}{\partial a} + \frac{\partial(f\dot{c})}{\partial c} \right] \, dadc \\ &= - \int_0^\infty \partial(f\dot{a}) \, dc - \int_0^\infty \partial(f\dot{c}) \, da. \end{aligned}$$

However as $a \rightarrow 0$ or $c \rightarrow 0$, the change in the number of particles is due to a disappearance of particles. Hence the change in the total number of particles in the system is

$$\frac{dN}{dt} = \lim_{a \rightarrow 0} (f\dot{a}) + \lim_{c \rightarrow 0} (f\dot{c}), \quad (5.21)$$

and is equal to the flux of particles at the origin.

The total volume of the solid particles in the system, from equations (5.1) and (5.20) is

$$\phi = \int_0^\infty 4\sqrt{3} \, a^2 c \, f(a, c, t) \, dadc. \quad (5.22)$$

The continuity equation (5.19) has to be solved in order to describe the behaviour of the system.

This requires expressions for \dot{a} and \dot{c} which are obtained by finding general expressions for the rate of mass transfer due to the diffusion process and the interfacial reaction process.

The rate of mass transfer by diffusion from the two hexagonal facets and the six prismatic facets are obtained by using Fick's first law for the diffusional flux of material. The flux J_s of material from the hexagonal or prismatic surface of a particle is defined as the number of moles of material crossing the corresponding surface-liquid interface per unit area per unit time. Employing Fick's first law yields

$$J_s = -D|\nabla C_s|,$$

which implies that

$$\frac{1}{A} \frac{dn}{dt} = -D\nabla C_s.$$

Substituting the expressions for the surface area of the hexagonal (eq.(5.2)) and prismatic (eq.(5.3)) facets for A and the ideal concentrations above the two facets in the expression above, the equations for the rate of mass transfer due to diffusion from the two hexagonal and six prismatic facets are

$$\dot{n}_{001} = -2 \times 2\sqrt{3} a^2 D \nabla C_{001},$$

and

$$\dot{n}_{100} = -6 \times \frac{4}{\sqrt{3}} acD \nabla C_{100},$$

where D is the diffusion coefficient and \dot{n}_{001} and \dot{n}_{100} are the number of moles transferred per unit time from the two crystal facets.

In the LSW theory [3, 4], the system consisted of a few particles which meant that the dimensions of the particles were much smaller compared to the distance between them. Based on this assumption the gradient of the ideal concentration above each facet is assumed to be of the form $\nabla C_{001} \approx \frac{C'_{001} - C}{c}$ and $\nabla C_{100} \approx \frac{C'_{100} - C}{a}$ respectively [4], where C'_{001} and C'_{100} are the actual concentrations above the (001) and the (100) facets and C is the average background concentration in the liquid medium. Therefore the two equations above simplify to give

$$\dot{n}_{001} = -2 \times 2\sqrt{3} \times \frac{a^2}{c} D (C'_{001} - C), \quad (5.23)$$

and

$$\dot{n}_{100} = -6 \times \frac{4}{\sqrt{3}} cD (C'_{100} - C). \quad (5.24)$$

The number of moles of material transferred per unit time by the interfacial reaction process is assumed to be proportional to the area of the interface and to the difference between the ideal and actual concentrations above the two facets, that is

$$\dot{n}_{001} = -2 \times 2\sqrt{3} a^2 k_{001} (C_{001} - C'_{001}), \quad (5.25)$$

and

$$\dot{n}_{100} = -6 \times \frac{4}{\sqrt{3}} ack_{100} (C_{100} - C'_{100}), \quad (5.26)$$

where k_{001} and k_{100} are the interfacial reaction constants associated with the hexagonal and prismatic facets respectively.

The rates of mass transfer due to the diffusion process and the interfacial reaction process on the hexagonal facets (eq.(5.23) and eq.(5.25)) and the prismatic facets (eq.(5.24) and eq.(5.26)) are equal in equilibrium. Hence expressions for C'_{001} and C'_{100} may be obtained:

$$C'_{001} = \frac{DC + ck_{001}C_{001}}{D + ck_{001}}, \quad (5.27)$$

and

$$C'_{100} = \frac{DC + ak_{100}C_{100}}{D + ak_{100}}. \quad (5.28)$$

Substituting eq.(5.27) into either eq.(5.23) or eq.(5.25), and eq.(5.28) into one of the equations (5.23) or (5.26) yields the general expressions for the rate of mass transfer from the hexagonal and prismatic surfaces:

$$\dot{n}_{001} = \frac{-4\sqrt{3} a^2 k_{001} D}{D + ck_{001}} (C_{001} - C), \quad (5.29)$$

and

$$\dot{n}_{100} = \frac{-8\sqrt{3} ack_{100} D}{D + ak_{100}} (C_{100} - C). \quad (5.30)$$

A geometrical argument relating the change in the number of moles in a particle with time to the rate at which the volume of a hexagonal particle changes with time is used to obtain expressions for the time derivatives of a and c . It follows from equations (5.5) and (5.1) that,

$$\frac{dn(a, c)}{dt} = \frac{1}{V_m} \left(8\sqrt{3} ac \frac{da}{dt} + 4\sqrt{3} a^2 \frac{dc}{dt} \right).$$

A change in the number of moles at the (001) surface corresponds to a change in c and a change in the number of moles at the (100) surface corresponds to a change in a . Therefore,

$$\dot{n}_{001} = \frac{1}{V_m} \frac{dV_{001}}{dt}$$

$$\begin{aligned}
&= \frac{4\sqrt{3}a^2}{V_m} \frac{dc}{dt} \\
&= \frac{-4\sqrt{3} a^2 D k_{001}}{D + ck_{001}} (C_{001} - C).
\end{aligned}$$

Rearranging the above equation and solving for \dot{c} gives

$$\dot{c} = \frac{-V_m D k_{001}}{D + ck_{001}} (C_{001} - C), \quad (5.31)$$

and similarly,

$$\dot{a} = \frac{-V_m D k_{100}}{D + ak_{100}} (C_{100} - C). \quad (5.32)$$

In a dilute medium, it is assumed that very little accumulation of mass occurs in the liquid medium. This means that as the small particles dissolve in the liquid medium, most of this mass diffuses through the liquid and precipitates onto the larger particles, and the approximation that the change in the concentration of the liquid medium with time is negligible is made:

$$\begin{aligned}
\frac{\partial C}{\partial t} &= - \int_0^\infty \dot{n}(a, c) f(a, c, t) dadc \\
&= - \int_0^\infty (8\sqrt{3} ac \dot{a} + 4\sqrt{3} a^2 \dot{c}) f(a, c, t) dadc \\
&\approx 0.
\end{aligned} \quad (5.33)$$

Substituting the equations (5.31), (5.32), (5.16) and (5.17) into eq.(5.33) yields an expression for the concentration in the liquid medium C :

$$\begin{aligned}
C &= \left[2k_{100}C_{100}^o \int_0^\infty \frac{ac}{D + ak_{100}} f(a, c, t) dadc + k_{001}C_{001}^o \int_0^\infty \frac{a^2}{D + ck_{001}} f(a, c, t) dadc \right. \\
&+ \frac{2k_{100}C_{100}^o V_m \sigma_{100}}{RT} \int_0^\infty \frac{c}{D + ak_{100}} f(a, c, t) dadc \\
&+ \left. \frac{2k_{100}C_{100}^o V_m \sigma_{001}}{RT} \int_0^\infty \frac{a}{D + ak_{100}} f(a, c, t) dadc \right]
\end{aligned}$$

$$\begin{aligned}
& + \frac{k_{001}C_{001}^o V_m \sigma_{100}}{RT} \int_0^\infty \frac{a}{D + ck_{001}} f(a, c, t) da dc \Big] \\
& \div \left[2k_{100} \int_0^\infty \frac{ac}{D + ak_{100}} f(a, c, t) da dc + k_{001} \int_0^\infty \frac{a^2}{D + ck_{001}} f(a, c, t) da dc \right]. \quad (5.34)
\end{aligned}$$

In a numerical solution to the problem, the approximation that the concentration of the liquid medium is constant need not be made as the equations of the ACT are solved selfconsistently to determine the grain growth of the system.

5.2 Diffusion-controlled and interfacial reaction-controlled processes

There are four cases that may be studied:

1. If $ck_{001} \gg D$ and $ak_{100} \gg D$, mass transfer is said to be diffusion controlled on the (001) and the (100) facets. Equations (5.31) and (5.32) simplify to

$$\dot{c} = \frac{-V_m D}{c} (C_{001} - C), \quad (5.35)$$

and

$$\dot{a} = \frac{-V_m D}{a} (C_{100} - C). \quad (5.36)$$

2. If $ck_{001} \ll D$ and $ak_{100} \ll D$, mass transfer is said to be controlled by the interfacial reaction.

It follows from equations (5.31) and (5.32) that

$$\dot{c} = -V_m k_{001} (C_{001} - C), \quad (5.37)$$

and

$$\dot{a} = -V_m k_{100} (C_{100} - C). \quad (5.38)$$

3. If $ck_{001} \gg D$ and $ak_{100} \ll D$, mass transfer is controlled by diffusion on the (001) surface and it is controlled by the interfacial reaction on the (100) surface. It follows from equations (5.31) and (5.32) that

$$\dot{c} = \frac{-V_m D}{c} (C_{001} - C), \quad (5.39)$$

and

$$\dot{a} = -V_m k_{100} (C_{100} - C). \quad (5.40)$$

4. If $ck_{001} \ll D$ and $ak_{100} \gg D$, mass transfer is controlled by the interfacial reaction on the hexagonal facets and by diffusion on the prismatic facets. Then the equations (5.31) and (5.32) simplify to

$$\dot{c} = -V_m k_{001} (C_{001} - C), \quad (5.41)$$

and

$$\dot{a} = \frac{-V_m D}{a} (C_{100} - C). \quad (5.42)$$

In principle, one has the ability to vary D by choosing different liquid media and hence a particular system, such as Si_3N_4 , may exhibit one or all of the above cases with different liquid phases.

5.3 Chemical isotropy and physical anisotropy

Physical anisotropy and chemical isotropy imply that a Si_3N_4 grain is a hexagonal prism, however the different facets of the grain have the same chemical properties. The system becomes chemically isotropic if the interfacial energies, the interfacial reaction constants and the saturation concentrations associated with the hexagonal and the prismatic facets are equal, that is

$$\begin{aligned}\sigma_{001} &= \sigma_{100} = \sigma \\ k_{001} &= k_{100} = k \\ C_{001}^o &= C_{100}^o = C^o\end{aligned}\tag{5.43}$$

In this limit, the expression for the concentration in the liquid medium (eq.(5.34)) reduces to

$$\frac{C}{C^o} = 1 + \frac{2k\sigma V_m}{RT} \frac{\int_0^\infty \frac{a f(a,c,t) da dc}{D+ck} + \frac{(a+c) f(a,c,t) da dc}{D+ak}}{\int_0^\infty \frac{a^2 f(a,c,t) da dc}{D+ck} + 2 \int_0^\infty \frac{ac f(a,c,t) da dc}{D+ak}}.\tag{5.44}$$

The critical lateral radius a^* and the critical longitudinal radius c^* are equal to each other in this limit and are given by the expression [4]

$$a^* = c^* = \frac{2 \int_0^\infty \frac{ac f(a,c,t) da dc}{D+ak} + \int_0^\infty \frac{a^2 f(a,c,t) da dc}{D+ck}}{\int_0^\infty \frac{(a+c) f(a,c,t) da dc}{D+ak} + \int_0^\infty \frac{a f(a,c,t) da dc}{D+ck}}.\tag{5.45}$$

By substituting eq.(5.43) and eq.(5.45) into the expressions for the ideal concentrations above the hexagonal and prismatic facets (eq.(5.16) and eq.(5.17)) it may be shown that the ideal

concentrations above the two different facets are equal when the system is chemically isotropic:

$$C_{001} = C^o \left[1 + \frac{2 \sigma V_m}{a^* RT} \right], \quad (5.46)$$

$$C_{100} = C^o \left[1 + \frac{2 \sigma V_m}{a^* RT} \right]. \quad (5.47)$$

Substituting equations (5.46), (5.47) and (5.44) into the equations (5.32) and (5.31) yields

$$\begin{aligned} \dot{a}(a^*, c^*, C) &= \dot{c}(a^*, c^*, C) \\ &= \frac{V_m D k C^o}{D + ck} \left[\left(1 + \frac{2 \sigma V_m}{a^* RT} \right) - \left(1 + \frac{2 \sigma V_m}{a^* RT} \right) \right] \\ &= 0. \end{aligned} \quad (5.48)$$

Thus the ACT collapses into the LSW theory in the limit of chemical isotropy and physical anisotropy.

5.4 Comparison between the model developed by Kitayama *et al* and the anisotropic coarsening theory

The model of anisotropic Ostwald ripening developed Kitayama *et al* [5] and the anisotropic coarsening theory are both general theories which describe anisotropic Ostwald ripening in an anisotropic system of particles such as completely faceted crystals. Numerical solutions of the basic equations describing these theories is used to model the anisotropic growth in an anisotropic system of particles. These models are applied to investigate the anisotropic coarsening of hexagonal β -Si₃N₄ (refer to fig.(3.1)) in a liquid medium.

In Kitayama's [5] model, the system consists of a finite number of discrete particles. The particles are described by two parameters $a(t)$ and $c(t)$ which represent the width and length of a particle at a time t . The grain growth behaviour of the particles in the system is determined by solving the equations (3.36), (3.37) and (3.39) selfconsistently. In the ACT, the system consists of a dilute dispersion of particles surrounded by a liquid medium, and is described in terms of a distribution function $f(a, c, t)$ (refer to eq.(5.18)) which is a function of the lateral radius a , the longitudinal radius c and time t . The distribution function satisfies a continuity equation (5.19) which conserves the number of particles in the system and allows for the particles disappearing by Ostwald ripening. The grain growth behaviour of the system in the ACT is determined by the evolution of the distribution function $f(a, c, t)$, and the evolution of the distribution function is obtained by solving the equations of the theory selfconsistently.

The driving force for mass transfer in both these models is a chemical potential gradient between the hexagonal and prismatic facets and the liquid medium. The expressions for the chemical potential on the hexagonal (eq.(3.31)) and prismatic (eq.3.32) facets in Kitayama *et al* [5] do not account for the different interfacial energies on the dissimilar facets, and in further investigations [21, 17] conducted the interfacial energies are still isotropic. In the ACT, the chemical potential expressions (eq.(5.12) and eq.(5.13)) take the different interfacial energies on the hexagonal and prismatic facets into account. Furthermore, the chemical potentials of the hexagonal and prismatic facets are related to the ideal concentrations (eq.(5.16) and eq.(5.17)) above these facets. This step introduces the saturation concentrations C_{001}^o and C_{100}^o of the respective facets into the equations eq.(5.32) and (5.31) through the equations (5.16) and (5.17).

The values of these saturation concentrations depend on the liquid medium and is an indication of the solubility on the different facets in the liquid medium.

By considering a discrete system of particles, Kitayama *et al* [5] avoid dealing with the numerical difficulties associated with the $1/a$ and $1/c$ terms in eq.(5.16) and eq.(5.17) as a and $c \rightarrow 0$, and the disappearance of particles from the system due to Ostwald ripening is not taken into account in their model.

Studies [1, 13, 22] have shown that the growth mechanism on the hexagonal facets are not isotropic, and that the growth rate on the hexagonal facet does not depend linearly on the concentration gradients for mass transfer due to the interfacial reaction process. Kitayama *et al* [5] assume that the growth mechanisms on the hexagonal and the prismatic facet are isotropic and no attempt to improve on this in later applications of the model [21, 17] has been made. The ACT also makes this assumption as a first approximation. However, in future applications of the theory a more realistic expression for eq.(5.25) which describes the growth rate of the hexagonal facet due to the interfacial reaction process, will be used in the numerical studies since the complete set of equations are solved selfconsistently to determine the grain growth behaviour of the system.

Chapter 6

Numerical Studies of the Anisotropic System

6.1 Numerical methodology

The numerical methods necessary for a stable solution to the anisotropic problem were developed by first studying the LSW theory applied to an isotropic system of spherical particles. However, due to the numerical instabilities that arose when studying the isotropic system, only a preliminary investigation of the anisotropic system was possible. The resolution of this problem is the subject of on-going work.

The anisotropic problem is a two dimensional flux-conservative initial value problem. The Lax finite differencing method is used to differentiate a discrete version of the continuity equation (5.19) to obtain the evolution of the particle size distribution function $f(a, c, t)$ with time. The calculation of the intermediate values of f at half-space and half-time steps,

$(a_{i+1/2}, c_{j+1/2}, t_{n+1/2})$, is more complicated in the two dimensional case. Hence the Two-Step Lax-Wendroff method was not used in our initial calculations. The indices i and j represent discrete points in space along the a and c directions respectively, n represents discrete points in time and $f_{i,j}^n$ represents $f(a_i, c_j, t_n)$.

The finite difference form of the left and right hand sides of (5.19) is

$$\frac{f_{i,j}^{n+1} - f_{i,j}^n}{\Delta t} = -\frac{1}{2\Delta} \left(f_{i+1,j}^n \dot{a}_{i+1} - f_{i-1,j}^n \dot{a}_{i-1} + f_{i,j+1}^n \dot{c}_{j+1} - f_{i,j-1}^n \dot{c}_{j-1} \right), \quad (6.1)$$

where $\Delta a = \Delta c = \Delta$ is chosen for convenience and

$$a_i = i\Delta \quad i = 0, 1, 2, \dots, I, \quad (6.2)$$

and

$$c_j = j\Delta \quad j = 0, 1, 2, \dots, J. \quad (6.3)$$

In the Lax method replacing the term $f_{i,j}^n$ by its average, $\frac{1}{4} (f_{i+1,j}^n + f_{i-1,j}^n + f_{i,j+1}^n + f_{i,j-1}^n)$, makes the method more stable [19]. Solving for $f_{i,j}^{n+1}$ yields

$$\begin{aligned} f_{i,j}^{n+1} &= \frac{1}{4} \left(f_{i+1,j}^n + f_{i-1,j}^n + f_{i,j+1}^n + f_{i,j-1}^n \right) \\ &\quad - \frac{\Delta t}{2\Delta} \left(f_{i+1,j}^n \dot{a}_{i+1} - f_{i-1,j}^n \dot{a}_{i-1} + f_{i,j+1}^n \dot{c}_{j+1} - f_{i,j-1}^n \dot{c}_{j-1} \right). \end{aligned} \quad (6.4)$$

If stable solutions are to be obtained using the Lax method, then it must satisfy the Courant

stability condition [19] which requires the time step to be of the form

$$\Delta t \leq \frac{\Delta}{\sqrt{2} \sqrt{(\dot{a}_i)^2 + (\dot{c}_j)^2}}, \quad (6.5)$$

for a two dimensional flux-conservative equation. The time step used in the calculations was chosen to be

$$\Delta t = \frac{0.8 \Delta}{\sqrt{2} \sqrt{(\dot{a}_1)^2 + (\dot{c}_1)^2}}. \quad (6.6)$$

The initial distribution function was chosen to be the product of two Gaussian functions. The change in the total number of particles (eq.(5.20)), the total volume of solid particles (eq.(5.22)) and the volume per particle with time and the growth exponents are calculated in the same manner as for the isotropic system.

Basic structure of the calculation

The structure for the calculation of the anisotropic system is given below:

1. Declare all constants and variables.
2. At $t = 0$:
 - Generate the initial distribution function $f(a_i, c_j, 0)$ and normalise it using (4.16).
 - Calculate:
 - the time step Δt using (6.6).

- the total volume of solid using (5.22) as a function of time,
- the concentration in the liquid medium using (5.34) as a function of time,
- \dot{a}_i and \dot{c}_j using (5.32 and 5.31) as a function of time, and

3. Loop over time:

- Calculate

- $\dot{a}_i \pm 1$ and $\dot{c}_j \pm 1$,
- $f_{i,j}^{n+1}$ using (6.4),
- the concentration in the liquid medium,
- the total volume, and
- the total number of particles in the system.

- Write out data to files.

4. Propagate the system until a steady state situation is attempted.

6.2 Results and discussion

6.2.1 Data used for modeling

The values for the fundamental parameters used in the calculations are obtained from references [5] and [1] and are listed in the table below:

Sintering temperature:	2123 K
Diffusion constant:	$D_o = 10^{-2} - 10^4 \text{ m}^2\text{s}^{-1}$, $Q = -545 \text{ kJmol}^{-1}$ $D = D_o \exp(Q/RT)$
Reaction constant:	$k_{100} = 9.9 \times 10^{-9} \text{ ms}^{-1}$
Interfacial energy:	$\sigma_{100} = 0.10 \text{ Jm}^{-2}$
Saturation:	$C_{100}^o = 1.3 \times 10^4 \text{ mol m}^{-3}$

Table 6.1: A table of the values of the fundamental parameters of Si_3N_4 used in the numerical study of the anisotropic system.

6.2.2 Preliminary results for the anisotropic system

The initial distribution function $f(a, c, t)$ for the anisotropic system of Si_3N_4 particles is obtained from the product of a Gaussian function depending on a with a Gaussian function depending on c . The graph below is obtained by plotting $f(a, c, t)$ against a and c .

Initial Distribution Function

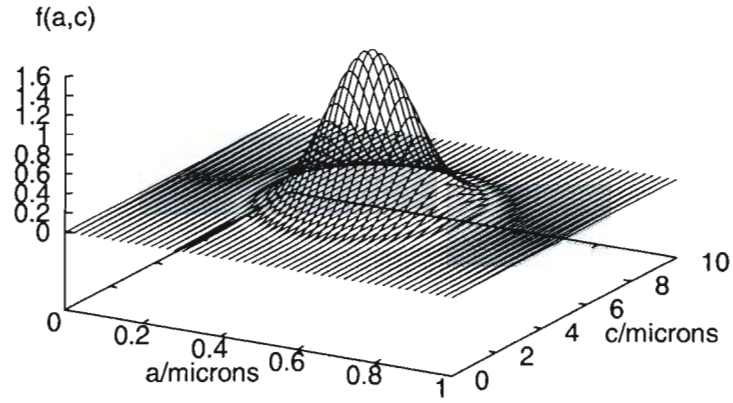


Figure 6.1: The initial distribution function of the anisotropic system.

The number of particles decreases as a function of time since particles disappear from the system as a result of the Ostwald ripening process.

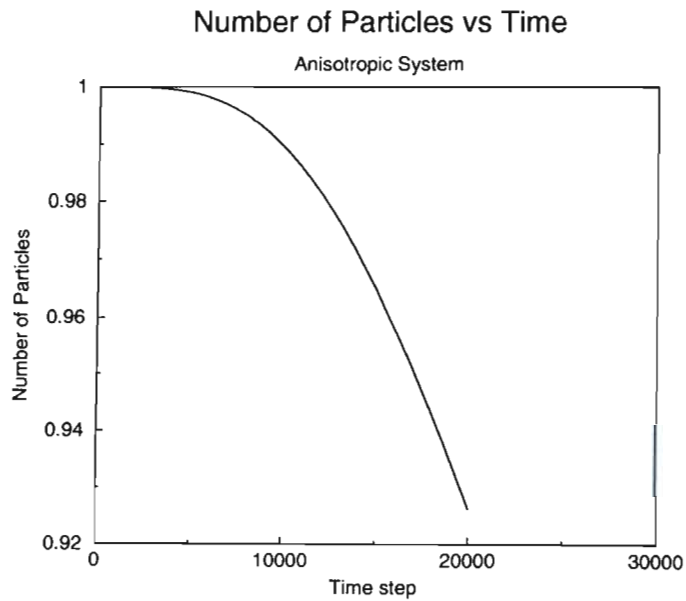


Figure 6.2: The change in the number of particles as a function of time.

The total volume of solid material in the system reaches a maximum value and then decreases as time increases.

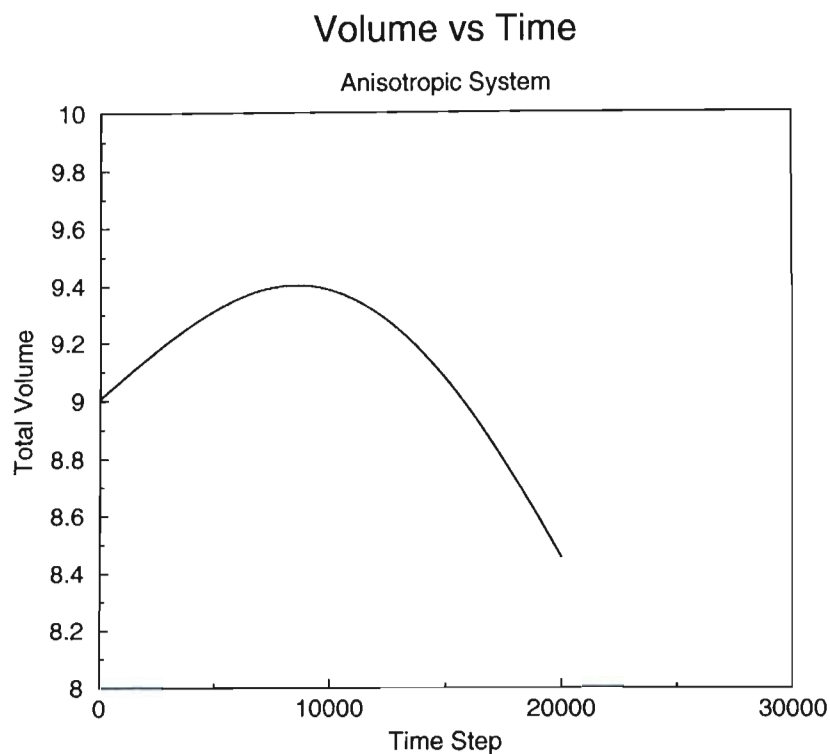


Figure 6.3: The total volume of solid particles in the anisotropic system as a function of time.

This is a new and interesting result which will be investigated further once the numerical instabilities associated with the isotropic system are understood, in order to determine the implications of this result if it is not an artifact of the calculation. If this is a real effect, then this could have profound implications on the understanding of the coarsening of anisotropic systems.

The behaviour of the volume per particle as a function of time is similar to the total volume of the particles in the system. It obtains a maximum value and then decreases as time increases.

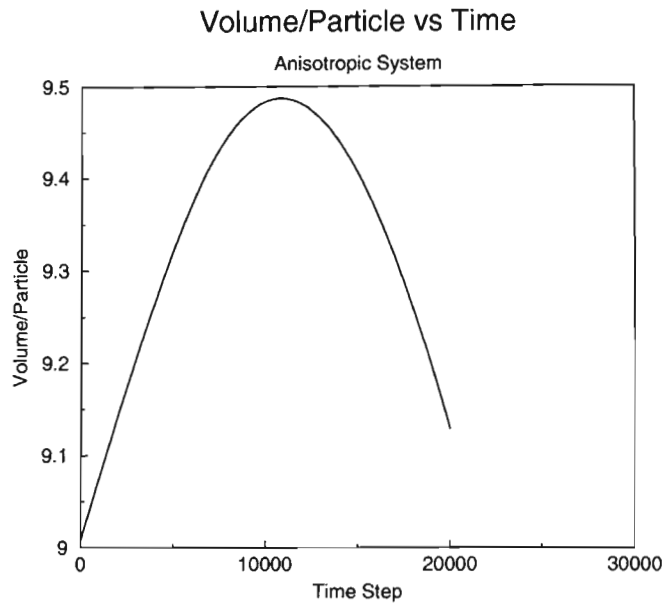


Figure 6.4: The volume per particle as a function of time for the anisotropic system.

Growth exponents are obtained by plotting the $(volume/particle)^{n/3}$ versus time for various values of n .

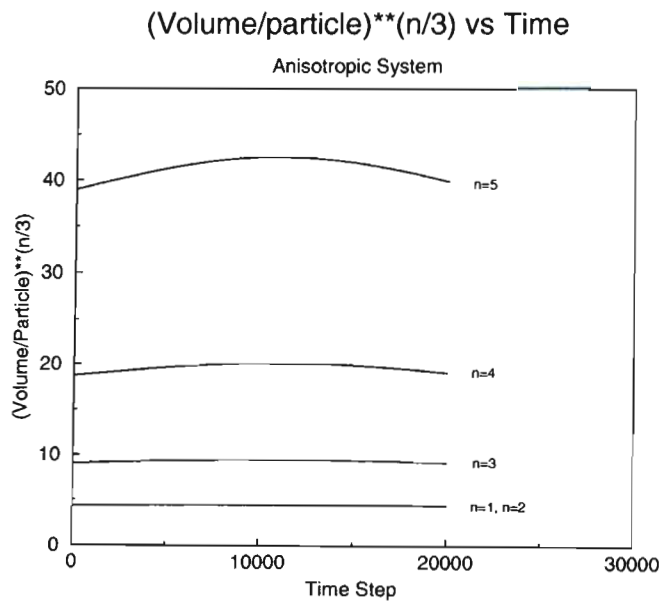


Figure 6.5: The $(volume/particle)^{n/3}$ as a function of time for the anisotropic system.

The numerical instabilities in the isotropic system arise from the $1/r$ singularity at the origin in eq.(3.10). In the anisotropic system, the $1/a$ and $1/c$ in equations (5.16) and (5.17) diverge as a and $c \rightarrow 0$, which indicate that small particles disappear at a very rapid rate which is the source of the instabilities in the calculations. Once the instabilities associated with the numerical solution of the isotropic problem are better understood, a more complete study of the anisotropic problem will be conducted. This is the subject of future studies.

6.3 Future directions

The efforts to understand the instabilities that have hampered the numerical solution to the isotropic and consequently the anisotropic problem is on-going, and a more complete study of the anisotropic problem forms the basis for a PhD study.

There are several phenomena that affect the grain growth behaviour of Si_3N_4 particles during sintering such as the α to β transformation for example, which have a significant influence on microstructural evolution. The anisotropic coarsening model may be extended to study and understand the effects of such phenomena on the grain growth behaviour of Si_3N_4 materials.

The purpose of theoretical models of coarsening are to provide qualitative and quantitative understanding of the coarsening (and the sintering) process. The current models have provided a more qualitative understanding of sintering in terms of the mechanisms, processing parameters (such as particle size, temperature and applied pressure) and fundamental parameters.

The lack of information on the fundamental parameters [9] such as interfacial energies, reaction concentrations and saturation concentrations make quantitative investigations very difficult at present. More careful measurements and calculations of these parameters are required if more accurate quantitative predictions are to be made.

The current models for grain growth of faceted crystals such as Si_3N_4 assume the surface energies of all crystal facets to be the same. Experimental investigations show that the growth rate on the prismatic facet of a Si_3N_4 particle (refer to fig.(5.1)) does not depend linearly on concentration gradients [22, 13] and that this has a significant influence on the evolution of the grain aspect ratios during sintering [22]. The advantage of numerical solutions is that these unrealistic assumptions are unnecessary, and the actual values of the surface energies for the different facets as well as the actual expressions describing the growth rates may be used in the model calculations.

The preliminary results on the change in the total volume with time in the isotropic and the anisotropic systems (refer to fig.(4.8) and fig.(6.3)) indicate that accumulation of mass in the liquid medium is not negligible as was assumed in the LSW theory [3, 4]. We would like to develop a finite element analysis solution to the problem since this would be a more realistic model of the system because the effect of the accumulation of mass in the liquid phase on grain growth may be studied. In addition, the effects of grain orientations relative to one another in the system and the effects of the diffusion and interfacial reaction constants on grain growth may also be studied. This will enable us to go beyond the dilute limit of our calculations.

The α - β transformation which occurs during liquid-phase sintering of Si_3N_4 has a significant influence on the final microstructure [5]. The present theory may be extended to account for this transformation.

Seeding of α - Si_3N_4 powders with a small amount of large, elongated β -nuclei has been used extensively to tailor the microstructure Si_3N_4 ceramics as a means of improving properties such as fracture toughness and strength. The presence of the β -nuclei affects the solubility of Si_3N_4 in the liquid medium which in turn influences the size and shapes which the grains achieve during liquid-phase sintering. We would like to apply the anisotropic coarsening theory to study the effects of seeding on the grain growth behaviour of Si_3N_4 particles.

Finally, we would like to apply this theory to study liquid-phase sintering of other anisotropic systems in the future, for example SiC which form hexagonal platelet structures.

Chapter 7

Conclusions and Final Remarks

We have formulated a new anisotropic coarsening theory applicable to anisotropic grain growth in a system of completely faceted crystals such as Si_3N_4 . It is a general theory. In the limit of chemical isotropy and physical anisotropy, the anisotropic theory collapses into the LSW theory.

The fact that small particles disappear at very rapid rates from the system gives rise to numerical instabilities in the numerical analysis of the LSW and anisotropic coarsening theories. Consequently, only preliminary numerical results for the evolution of the distribution function and growth exponents are presented in this thesis.

Numerical analysis of coarsening is a relatively new technique compared to the frequently used analytical methods. As a result, the numerical instabilities that arise from the $1/r$ term as $r \rightarrow 0$ in eq.(3.10) – regardless of the numerical method used to solve the continuity equation (3.5) – have not been dealt with in the literature in previous numerical studies of Ostwald ripening. This is one of the factors that has caused the progress in the understanding of the

numerical instabilities to be very difficult and slow. The efforts to overcome these numerical difficulties are on-going.

Numerical difficulties aside, a numerical solution to the problem of Ostwald ripening in isotropic and anisotropic systems is more accurate and realistic compared to other analytical techniques [9]. The approximations made in the LSW theory, which were made out of convenience to obtain an analytical solution to the problem, are unnecessary since the exact equations of both the LSW and anisotropic coarsening theories may be solved self-consistently without having to make approximations.

The anisotropic coarsening theory has numerous fundamental parameters such as the surface energies, diffusion and interfacial reaction constants, and the saturation concentrations C_{100}^o and C_{001}^o . The values for the surface energies and diffusion and interfacial reaction constants used in our calculations were selected from data used by Kitayama *et al* [5] and Herrmann [1]. The purpose of theoretical models of sintering are to provide qualitative and quantitative understanding of the sintering process. The current models have provided more qualitative understanding of sintering in terms of the mechanisms, processing parameters (such as particle size, temperature and applied pressure) and fundamental parameters. The lack of information on these fundamental parameters [9] makes quantitative investigations difficult at present. More careful measurements and calculations of these parameters are required if more accurate quantitative predictions are to be made.

The current models for grain growth of faceted crystals such as Si_3N_4 are based on isotropic surface energies and growth rates [1]. This assumption is unnecessary, and the actual values of the surface energies for the different facets must be used in the model calculations.

Future applications of the anisotropic coarsening theory to hexagonal Si_3N_4 particles involve:

- including expressions for growth rates which do not depend linearly on concentration gradients in numerical calculations to model the growth behaviour more accurately and realistically,
- developing a finite element analysis of the problem in which the effects of the accumulation of mass in the liquid medium and grain impingement on grain growth may be studied,
- extending the anisotropic theory to account for the α to β transformation which occurs during liquid-phase sintering of Si_3N_4 materials and which has a significant influence on grain growth, and
- studying the effects of seeding on the evolution of grain size distributions and aspect ratios.

We plan to apply the anisotropic coarsening theory to study coarsening in other faceted crystals such as silicon carbide.

This will be the basis of a PhD study.

Glossary of Technical Terms

Additives: Compounds that are added in low concentrations to the ceramic powder prior to sintering to control microstructural evolution and to improve the sintering process.

Agglomerate: A cluster of particles which are held together by weak surface bonds or by liquid and solid bridges.

Amorphous: Devoid of crystalline form. Amorphous materials lack a regular arrangement of their constitutive atoms.

Annealing: An isothermal heat treatment which is administered to ceramic materials to reduce thermal stresses within the compact or to change the chemical composition of the microstructure. Annealing temperatures are high but are lower than sintering temperatures.

Aspect ratio: The ratio of grain length to grain width.

Attrition milling: A milling technique which uses balls as the grinding media. The material to be milled and the grinding media are stirred vigorously with a rotating stirrer within a milling chamber. The frequency of the stirrer varies between 1 Hz and 10 Hz.

Axial pressing: A consolidation method in which pressure is applied along a particular di-

rection (or axis) to a powder compact in a die.

Ball milling: A milling technique which uses balls as the grinding medium. The balls are made to collide with the starting material, and finer particles are obtained in this manner.

Binder: A processing additive which strengthens the green body, provides plasticity in feed material for the plastic-forming shaping methods and helps to produce a granular feed material for the pressing methods. Long-chain organic polymers are often used as binders.

Burnout: The heat treatment which is used to remove processing additives from the green body prior to sintering.

Capsule HIP: A powder compact is encapsulated in a deformable metal container referred to as a can and then densified by HIP.

Carbothermal reduction: Si_3N_4 is produced by the carbothermal reduction of SiO_2 by carbon at approximately 1500°C .

Casting: Consolidation techniques which involve consolidation of powders from a slurry. In general, these methods are used to produce relatively thin green bodies. Slip casting and tape casting are examples casting techniques.

Ceramics: Inorganic, nonmetallic compounds that are, in general, crystalline and are formed between metallic and nonmetallic elements such as silicon and nitrogen (Si_3N_4) and aluminium and oxygen (Al_2O_3).

Coarsening: The growth mechanism which results in grain growth and pore growth without an increase in the density of the ceramic.

Cold pressing: A powder shaping technique in which pressure is applied uniaxially to the powder in a die and is used to shape the powder.

Colloidal methods: Powder shaping methods in which a mould is obtained from concentrated suspensions of particles in a liquid by allowing the particles in the suspension to settle into a shape under the influence of gravity or by centrifuging.

Composites: A second phase is added to a ceramic to improve the properties of the ceramic, for example, SiC fibres are added as a reinforcing phase to Al_2O_3 to improve the strength of the Al_2O_3 sample.

Creep: The gradual change in the shape of grains as a means of relieving compressive stresses within the ceramic sample.

De-agglomeration: The process in which the bonds between the agglomerated particles are broken yielding smaller individual particles.

Densification: The growth mechanism which is responsible for grain growth and an increase in the density of the ceramic.

Dispersant: Processing additives which are used to stabilize slurries by increasing the repulsion between the particles. Dispersants influence the viscosity of the slurries.

Extrusion: A powder shaping technique in which a stiff feed material is shaped by forcing it through a nozzle.

Feed material: The material that is shaped into a green body by the various shaping techniques. The feed material consists of a homogeneous distribution of the ceramic particles,

sintering and processing additives, and must have the required viscosity, plasticity and flexibility for shaping.

Finishing: A stage in the ceramic fabrication process in which the ceramic sample (either the green body or the sintered sample) are cut, polished or ground so that they meet specific requirements.

Fracture toughness: A property of a ceramic material which determines the strength of the ceramic. Fracture toughness depends on the grain shapes and sizes and on the composition of the grain boundary phase.

Furnace: An apparatus used to heat powder compacts to the sintering temperatures. Heat is generated by a furnace element such as a current-carrying resistor.

Gas-pressure sintering: A pressureless sintering technique in which a small external pressure is applied with the aid of a gas to prevent the powder compact from decomposing at the sintering temperatures.

Grain boundary: The region which separates grains in a ceramic compact. In polycrystalline materials, grain boundaries are areas where the periodic arrangement of the atoms is disrupted, and consequently the atoms in this region have a higher energy compared to atoms within the bulk.

Green body: The shaped, unsintered ceramic.

Green density: The density of a green body. It includes the sum of the pore volume and the volume occupied by the solid particles in the compact.

Grinding: A finishing technique in which friction is used to smoothen the surfaces of the ceramic sample.

Growth rate: The rate at which mass is added or removed from the surface of a particle.

Hard agglomerates: Clusters of particles that are bonded together chemically by solid bridges.

Hardness: The ability of a ceramic to withstand high pressures. Hardness may be determined by how easily it is to scratch or dent the surfaces of a ceramic sample.

Heating rate: The amount by which the temperature is change in a unit of time during the sintering process.

High-temperature properties: The behaviour of ceramic material above the temperature at which the grain boundary phase begins to weaken.

Hot pressing: A pressure sintering technique in which pressure is applied uniaxially to the powder in a die. Applied pressure may be as high as 40 MPa and only samples with simple geometries may be obtained.

Hot isostatic pressing: A form of pressure sintering in which pressure is applied isostatically to the powder in a pressure vessel with the aid of a gas. Applied pressures of up to 200 MPa are possible, and the samples with complex geometries may be obtained.

Impurity: These are elements or compounds that contaminate the ceramic powder. They are introduced into powders at any stage in the ceramic fabrication process, for example, as by-products of powder synthesis or during milling if the grinding medium is not the same as the ceramic material being milled. Impurities are one of the sources of defects during sintering.

Inclusion: A second phase within a ceramic compact which is added to the ceramic powder prior to sintering as a reinforcing phase (e.g. fibre-reinforcement) or which forms during sintering by unfavourable reactions between impurities and sintering additives for example, and which have a negative influence on the properties of the ceramic.

Injection moulding: A shaping technique in which the feed material is transported in to an injection chamber where it is heated to produce a viscous mass and then injected under pressure into a mould cavity. Once the mould cools the solid object is ejected from the mould cavity.

Isostatic pressing: A powder shaping technique which applies a uniform hydrostatic pressure to a powder contained in a rubber container.

Liquid-phase sintering: A sintering method in which sintering additives form a liquid at sintering temperatures which enhances mass transport rates and reduces sintering times.

Microstructural design The tailoring of microstructures to improve the properties of ceramic materials.

Microstructure: The structure of a ceramic that is visible with the aid of microscopes such as the scanning electron microscope.

Milling: A mechanical technique that uses mechanical forces such as collision, shear and compression to reduce particle sizes. Milling media such as balls or rods are made to collide with the material to be milled within a milling chamber by rotating or vibrating the chamber or by stirring the two components within the milling chamber.

Neck: The region of contact between adjacent particles in a compact which has a lower chemical potential compared to the particle surfaces. As a result mass tends to accumulate at the neck.

Nitridation: The reaction between metallic silicon and nitrogen at temperatures between 1200 and 1400 °C to produce Si_3N_4 .

Plasticiser: Processing additives that are used to soften the binder in the preparation of a feed material. Low molecular weight organic compounds are used as plasticizers.

Plastic-forming: Powder consolidation methods in which a mouldable feed material is deformed plastically. Injection moulding and extrusion are examples of plastic forming methods.

Polishing: A finishing technique which is used to refine or smoothen the surfaces of a ceramic sample.

Polycrystalline: A large crystalline material which is composed of numerous smaller crystallites separated by grain boundaries.

Pore: The spaces (or interstices) between particles in a compact. They are filled with a vapour phase or gases from the sintering atmosphere during sintering. The structure of the pores changes during sintering as a result of densification.

Porosity: The volume occupied by the pore in a powder compact.

Powder processing: The first stage in the ceramic fabrication process which produces ceramic powders with specific characteristics.

Pressing: Refers to the consolidation of ceramic powders in a die by the application of pressure.

Pressure sintering: An external pressure in the range of 40 MPa to 200 MPa is applied during sintering of a ceramic powder compact to enhance densification rates.

Pressureless sintering: Refers to the conventional sintering techniques used to sinter powder compacts. External pressures of up to 20 MPa may be applied during sintering.

Processing additive: Organic polymers that are mixed into the ceramic powder in small quantities to produce a suitable feed material for shaping in order to control the properties of the green body such as uniform particle packing and density.

Rearrangement: The movement of particles into more stable, densely packed positions during liquid-phase sintering. The force of the liquid medium on the grains in a compact causes rearrangement.

Room-temperature properties: In ceramics room temperature refers to the temperatures below the temperature at which the grain boundary phase begins to weaken. Thus room-temperature properties refer to the behaviour of the ceramics below that critical temperature.

Shaping: The second stage in the ceramic fabrication process in which ceramic powders are moulded into specific shapes that are referred to as green bodies.

Shrinkage: The change in the dimensions (such as length) of a compact during sintering divided by the initial value (that is, the value before sintering) of these dimensions.

Sintering: A heat treatment which causes particles in a green body to bond together to form a dense, solid ceramic by mass transfer between particles.

Sintering additive: An inorganic compound which is mixed into the ceramic powder and is used to enhance densification rates or to control grain growth.

Sintering atmosphere: The atmosphere which surrounds the powder compact during sintering for example, nitrogen, carbon monoxide, inert gases such as helium and argon and vacuum. Chemical reactions between the gas and the powder system, and the solubility of the gases in the powder have a significant influence on the ability to achieve high densities and controlled grain sizes.

Slip casting: A slurry is poured into a plaster of paris mould which contains micropores. The liquid from the slurry drains out slowly through the pores by an action similar to capillary rise leaving behind a consolidated layer of solid referred to as a cast. Once the cast of sufficient thickness forms, the excess slurry is removed and the cast is dried.

Slurry: A suspension of particles in a solvent which is used as the feed material for the casting methods.

Soft agglomerates: Clusters of particles that are held together by weak van der Waals forces.

Solid-state sintering: A type of sintering in which grain growth occurs as mass in the solid state is transferred between particles in the system.

Solvent: An organic liquid in which processing additives are dissolved before they are mixed into the ceramic powder. Water may be used as a solvent.

Starting material: The unprocessed ceramic material from which the ceramic powder is obtained.

Strength: A measure of the ability of ceramics to withstand the application of (compressive, tensile or shear) stresses. The strength of ceramics is proportional to the fracture toughness and inversely proportional to the square root of the defect size in the ceramic compact.

Suspension: Solid particles are dispersed in general in a liquid medium and prevented from settling to the bottom of the container by viscosity of the liquid and the forces between the particles in the system.

Tape casting: A casting technique in which the slurry is spread over a removable sheet of paper or plastic with the aid of a blade referred to as a doctor blade. Once dry, the tape is peeled from the surface and cut into the desired shapes.

Technical ceramics: Refer to ceramics that have, in general, been produced within the last 50 years and are used in electrical, magnetic and optical applications as well as in structural applications where high strength over a wide range of temperatures is required.

Theoretical density: The density of the ceramic material that may be obtained if all the pores in the ceramic sample have been completely filled with mass.

Whiskers: Short single-crystal fibres with aspect ratios in the range 15 to 20. These are used in microstructural engineering to increase the fracture toughness and strength of ceramics.

Acknowledgements

There are no words which adequately express how grateful I am to my supervisor, Dr Nithaya Chetty, for his involvement in my M.Sc. degree. His foresight and guidance are at the heart of the progress which I made in the last two years, and I deeply appreciate his constant encouragement.

I am also indebted to Dr Mathias Herrmann of the Fraunhofer Institute for Ceramic Technologies and Sintered Materials in Germany for suggesting the topic of coarsening and for his invaluable and ever-willing assistance and guidance.

I would like to thank my friends Mitchell de Bruyn and Frank Ortmann for helping me learn about all things computational, the physics M.Sc. students and Antionette Vorster for their company, encouragement and support. I wish to also thank my family (especially Mandira and Mahendra) for their support, and my beloved Guru ji for His guidance and encouragement.

Finally, I wish to express my appreciation to De Beers for the financial support of this Master's degree.

Resumé

Trisha Salagaram was born in Durban on 10 July 1978. She attended the university of Natal in Pietermaritzburg, and obtained a B.Sc. degree in 1999, majoring in physics and chemistry. In 2000 she obtained an Honours degree in physics. She completes a M.Sc. degree at the end of 2002.

Bibliography

- [1] M. Herrmann. Private Communication.
- [2] G. Petzow and M. Herrmann. Silicon Nitride Ceramics. *Structure and Bonding*, 102:47–148, 2002.
- [3] I. M. Lifshitz and V. V. Slyozov. The Kinetics of Precipitation from Supersaturated Solid Solutions. *J. Phys. Chem. Solids*, 19(1/2):35–50, 1961.
- [4] C. Wagner. Theorie der Alternung von Niederschlägen durch Umlösen (Ostwald-Reifung). *Z. Electrochem*, 65:581–591, 1961.
- [5] M. Kitayama et al. Modelling and Simulation of Grain Growth in Si_3N_4 - 1. Anisotropic Ostwald Ripening. *Acta Mater.*, 46(18):6541–6550, 1998.
- [6] H. Lange et al. Silicon Nitride—From Powder Synthesis to Ceramic Materials. *Angew. Chem. Int. Ed. Engl.*, 30:1579–1597, 1991.
- [7] F. L. Riley. Silicon Nitride and Related Materials. *J. Am. Cer. Soc.*, 83(2):245–262, 2000.
- [8] G. Ziegler et al. Review Relationships between Processing, Microstructure and Properties of Dense and Reaction-bonded Silicon Nitride. *J. Mat. Sci.*, 22:3041–3083, 1987.

- [9] M. N. Rahaman. *Ceramic Processing and Sintering*. Marcel Dekker, 270 Madison Avenue, New York, 1995.
- [10] E. Kroke. High-Pressure Synthesis of Novel Binary Nitrogen Compounds of Main Group Elements. *Angew. Chem. Int. Ed*, 41(1):77–82, 2002.
- [11] M. Schwarz et al. Spinel-Si₃N₄: Multi-Anvil Press Synthesis and Structural Refinement. *Adv. Mater.*, 12(12):883–887, 2000.
- [12] A. Zerr et al. Elastic Moduli and Hardness of Cubic Silicon Nitride. *J. Am. Cer. Soc.*, 85(1):86–90, 2002.
- [13] R. Riedel, editor. *Handbook of Ceramic Materials*. Wiley–VCH, Weinheim, 2000.
- [14] C. N. R. Rao, editor. *Chemistry of Advanced Materials*. Blackwell Scientific Publications, Oxford, 1993.
- [15] H. Björkland et al. β -Si₃N₄ Grain Growth, Part i: Effect of Metal Oxide Sintering Additives. *J. Eur. Cer. Soc.*, 17:1285–1299, 1997.
- [16] H. Björkland and L. K. L. Falk. β -Si₃N₄ Grain Growth, Part ii: Intergranular Glass Chemistry. *J. Eur. Cer. Soc.*, 17:1301–1308, 1997.
- [17] M. Kitayama et al. Modelling and Simulation of Grain Growth in Si₃N₄ -3. Tip Shape Evolution. *Acta Mater.*, 48(18-19):4635–4640, 1998.
- [18] P. W. Voorhees. Ostwald Ripening of Two-Phase Mixtures. *Annu. Rep. Mater. Sci.*, pages 197–214, 1992.

- [19] W. H. Press et al. *Numerical Recipes in FORTRAN*. Cambridge University Press, New York, New York, USA, second edition, 1992.
- [20] H. A. Atwater and C. M. Yang. Island Growth and Coarsening in Thin Films—Conservative and Nonconservative Systems. *J. Appl. Phys.*, 67(10):6202–6213, 1990.
- [21] M. Kitayama et al. Modelling and Simulation of Grain Growth in Si_3N_4 -2. The $\alpha - \beta$ Transformation. *Acta Mater.*, 46(18):6551–6557, 1998.
- [22] M. Herrmann et al. Some New of Microstructural Design of β - Si_3N_4 Ceramics. *Z. Metallkd.*, 92(7):788–795, 2001.
- [23] R. M. German. *Sintering Theory and Practice*. John Wiley and Sons, 1996.
- [24] J. S. Reed, editor. *Principles of Ceramic Processing*. John Wiley and Sons, Inc., New York, 1995.
- [25] D. R. Uhlmann W. D. Kingery, H. K. Bowen. *Introduction to Ceramics*. John Wiley and Sons, Inc., New York, second edition, 1976.
- [26] N. Hirosaki and Y. Akimune. Effect of Grain Growth of β -Silicon Nitride on Strength, Weibull Modulus, and Fracture Toughness. *J. Am. Cer. Soc.*, 76(7):1892–1894, 1993.
- [27] G. Pezzoti and M. Sakai. Effect of a Silicon Carbide "Nano-Dispersion" on the Mechanical Properties of Silicon Nitride. *J. Am. Cer. Soc.*, 77(11):3039–3041, 1994.
- [28] H-J Kleebe et al. Microstructure and Fracture Toughness of Si_3N_4 Ceramics: Combined Roles of Grain Morphology and Secondary Phase Chemistry. *J. Am. Cer. Soc.*, 82(7):1857–1867, 1999.

- [29] C. J. Lee and D. J. Kim. Effect of α - Si_3N_4 Particle Size on the Evolution of Si_3N_4 Ceramics. *J. Am. Cer. Soc.*, 82(3):753–756, 1999.
- [30] I. Tanaka et al. Impurity-Enhanced Intergranular Cavity Formation in Silicon Nitride at High Temperatures. *J. Am. Cer. Soc.*, 74(4):752–759, 1991.
- [31] D. S. Jacobs and I. W. Chen. Mechanica and Environmental Factors in the Cyclic and Static Fatigue of Silicon Nitride. *J. Am. Cer. Soc.*, 77(5):1153–1161, 1994.